# Testing Competing Caldera Models using U/Pb Geochronology; Intrusive History of the Questa Caldera: Latir Volcanic Field, New Mexico, USA

Michael J. Tappa

A thesis submitted to the faculty of the University of North Carolina at Chapel Hill in partial fulfillment of requirements for the degree of Master of Science in the Department of Geological Sciences

Chapel Hill
2009

Approved by:
Dr. Drew Coleman
Dr. Allen Glazner
Dr. Lara Wagner

# ABSTRACT

**MICHAEL J. TAPPA**: **Testing Competing Caldera Models using U/Pb Geochronology; Intrusive History of the Questa Caldera: Latir Volcanic Field, New Mexico, USA**
**(Under the direction of Drew Coleman)**

A compelling new model for caldera evolution challenges the standard depiction of large-scale volcanism. Here, I test these competing models by establishing the temporal and chemical relationship between ignimbrite and potential cogenetic plutons related to the Questa caldera, Latir volcanic field, New Mexico.

Results from zircon U/Pb geochronology indicate that the majority of intrusive rocks formed after ignimbrite eruption. The Rio Hondo pluton was assembled over a minimum of 500 k.y., and crystallization progressed from the structurally highest levels downward, consistent with top-down incremental assembly of the pluton. Trace-element modeling demonstrates that the plutonic rocks are not the residua of crystal fractionation, and the predicted systematic difference in trace-element chemistries of plutonic and volcanic rocks is not observed. Finally, the data presented here mostly support the new model for caldera evolution and is broadly inconsistent with the standard caldera model.

## ACKNOWLEDGEMENTS

I would like to thank Drew Coleman for all of the advice and support through this entire process. Field work could not have been conducted without the help of collaborator Matt Zimmerer; at the very least it would have been a lot less enjoyable. I would like to acknowledge Peter Lipman as the driving force behind this work. This manuscript, including the data it contains, was significantly improved because of Jesse Davis and his consistent willingness to assist either in the lab, with stimulating discussion, or by providing great music. Thanks to Russ Mapes, Ryan Mills, Sabrina Belknap, John Gracely, Scott Bennett, Breck Johnson, and all the other graduate students along the way who helped make the experience more enjoyable in too many ways to list. Funding was graciously provided by Ren Thompson of the U.S.G.S. and the UNC Martin Fund. Finally, I would like to thank my family for their constant unwavering support and love.

# TABLE OF CONTENTS

Page

# LIST OF TABLES

# LIST OF FIGURES

# 1. INTRODUCTION

Debate persists on the nature of the relationship between plutonic and volcanic rocks (e.g. de Silva et al., 2007). Opposing views propose that either plutonic rocks represent the unerupted crystal cumulates of volcanic eruptions and are thus complementary to volcanic rocks (Hildreth 2004; Eichelberger et al., 2006; Bachmann et al., 2007a; Lipman, 2007; de Silva and Gosnold, 2007), or that plutonic rocks are essentially unerupted equivalents of volcanic rocks (Glazner, 1991; Glazner et al., 2008). Large-scale (>100 $km^3$) caldera eruptions represent one end-member in the discussion of plutonic/volcanic rock connections because current caldera models predict voluminous pluton formation, up to an order of magnitude larger than the erupted material, during ignimbrite eruption (e.g. Lipman, 2007).

Traditional thought interprets caldera collapse and ignimbrite eruption to result from the partial evacuation of massive differentiated magma chambers at shallow crustal levels, the residuum of which is preserved as plutons (herein referred to as the "pluton-building model"; Smith, 1979; Lipman, 1984; Bachmann et al., 2000; Bachmann et al., 2002; Hildreth, 2004; Lipman, 2007). The pluton-building model is built, in part, by noting the similarity between zoning of large ignimbrites and zoning of intrusive suites such as the Tuolumne Intrusive Suite of the Sierra Nevada batholith (Hildreth, 1981). However, recently published geochronologic data and petrologic evidence show some plutonic systems (including the Tuolumne Intrusive Suite) that were previously thought to be the remnants of now eroded ignimbrites never existed as single large chambers in

the upper crust (Glazner et al.; 2004). Rather, plutons in the Tuolumne and elsewhere were emplaced incrementally and amalgamated over millions of years (Coleman et al., 2004; Matzel et al., 2006; Gracely, 2007). If mapped plutons never existed as massive single chambers, they cannot fractionate the voluminous siliceous cap the traditional caldera model requires to form ignimbrites. Consequently, there may be a disconnect between pluton-building events and ignimbrite eruptions (Glazner, 1991), and the traditional caldera model needs to be reevaluated.

In light of geochronologic data, Glazner et al. (2004) recognized that not all voluminous plutons are associated with ignimbrite eruptions, and further suggest that ignimbrite eruptions may not result in voluminous pluton formation. Their model, herein referred to as the "non-pluton-building model", predicts caldera collapse to result from a period of high magma flux to upper crustal levels forming a shallow laccolithic magma body that is unstable in the upper crust and collapses quickly after rapid amalgamation. In the non-pluton-building model, the chamber evacuates almost entirely, leaving few remnant plutonic rocks (Roche and Druitt, 2001; Glazner et al., 2004).

There are two fundamental differences between pluton-building and non-pluton-building models for formation of ignimbrites. First, the pluton-building model predicts massive remnant coeval plutons approximately three to ten times the volume of the ignimbrite (Smith, 1979; Bachmann et al., 2002; Hildreth, 2004; White et al., 2006; Lipman, 2007). In contrast, the non-pluton-building model predicts ignimbrites to be the erupted products of magma chambers that are comparable in size to the erupted material that erupt nearly completely leaving little, if any, plutonic residue (Fig 1.1-A).

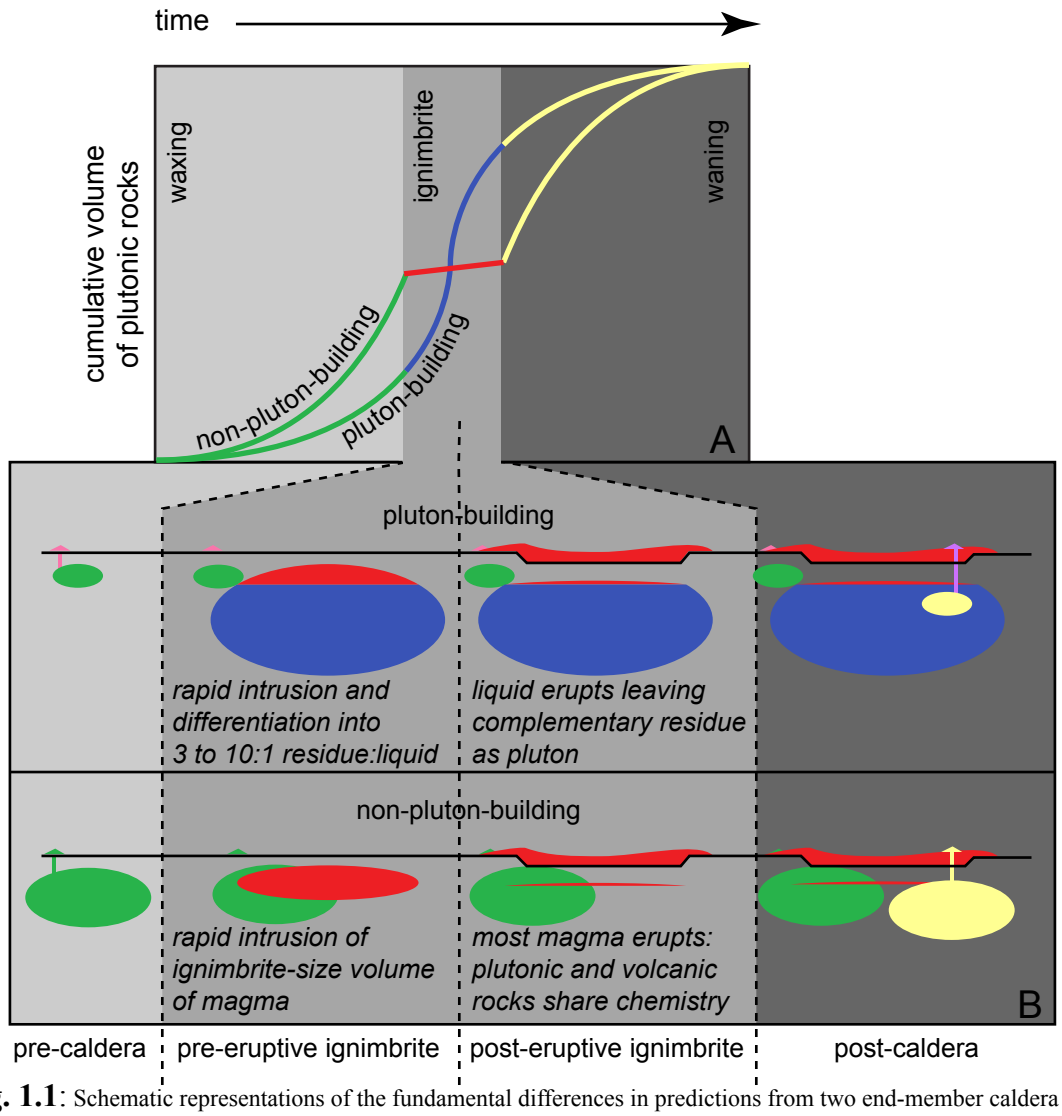


**Fig. 1.1**: Schematic representations of the fundamental differences in predictions from two end-member caldera models (pluton-building and non-pluton-building). Pre-caldera and post-caldera stages are synonymous with "waxing" and "waning" stages defined by Lipman (2007). Time progress to the right on the horizontal axis and is roughly to scale in (A) while the ignimbrite stage is exaggerated in (B). A) A plot of predicted cumulative plutonic rock volume through time from the two end-member caldera models. Colors correlate to plutonic rocks formed during different stages. Green represents pre-caldera, blue and red respectively represent the pluton-building and non-pluton-building ignimbrite stage, and yellow represents the post-caldera stage. In both models the final volume of plutonic rocks is identical, but the timing of pluton growth differs. The pluton-building end-member predicts formation of voluminous plutonic rock coincident with ignimbrite eruption. The non-pluton-building end-member predicts that the source magma chamber evacuates nearly completely during ignimbrite eruption, thus few plutonic rocks form during the ignimbrite stage and instead, most plutonic rocks form during the pre-caldera and post-caldera stages. B) Cross-sectional diagram demonstrating the two end-member predictions of chemical relations between plutonic and volcanic rocks. The ignimbrite stage was expanded and divided to demonstrate the end member's predictions immediately prior to and following caldera collapse. The colors for the plutonic rocks represent different stages and correlate to part A. For the pluton-building model the volcanic rocks are red to pink, whereas for the non-pluton-building model the volcanic rocks are the same colors as the plutonic rocks. The ignimbrite (both erupted and unerupted portions) is red in both models. The pluton-building end-member predicts magma that generates the ignimbrite, and other volcanic rocks, forms at the top of large chambers and is derived from magma differentiation. This process results in different, but complementary, chemistries for volcanic and plutonic rocks. The non-pluton-building model predicts that magma chamber differentiation does not significantly influence the chemistry of volcanic and plutonic rocks. Instead, plutonic rocks represent unerupted volcanic rocks, so the chemistry of coeval rocks should be equivalent.

A second distinction between the pluton- and non-pluton-building models is in the geochemical relation between plutonic and volcanic rocks. The pluton-building model predicts that ignimbrites form via differentiation processes within voluminous "big tank" magma chambers. Consequently, the residual plutonic rocks should be chemically complementarily to the ignimbrite (residue and liquid, respectively). The non-pluton-building model predicts that shallow crustal magma chamber differentiation does not significantly influence the chemistry of ignimbrites or plutonic rocks, and chemically the rocks should be identical if derived from similar sources (Fig 1.1-B).

Testing these competing hypotheses requires the uncommon exposure of both plutonic and volcanic rocks related to the same caldera. The atypical setting of the Questa caldera, located on the flank of the Rio Grande Rift, results in the exposure of ignimbrite and related plutonic rocks. With detailed high-precision geochronology of the Questa plutonic and volcanic rocks, in should be possible to determine if they formed contemporaneously. If contemporaneous plutonic/volcanic rock pairs are identified it should be possible to evaluate whether they plausibly are complementary residue and liquid compositions, or they share similar chemistries. Independent of identifying plutonic/volcanic rock pairs, it should also be possible to test whether the timing of magma intrusion and geochemical evolution of the plutons is consistent with formation of magmas similar to the erupted rocks.

# 2. GEOLOGIC BACKGROUND

The Questa caldera, located in the Latir volcanic field of north-central New Mexico, formed in response to eruption of the Amalia Tuff (Lipman et al., 1986). The Latir field is ideal for examining plutonic/volcanic connections because it has a simple eruptive history, and asymmetric uplift along the Rio Grande rift exposes subvolcanic plutons while preserving volcanic rocks including the Amalia Tuff (Lipman, 1984).

The Latir volcanic field comprises the southern margin of the Southern Rocky Mountain volcanic field, a volcanic province that hosts multiple Oligocene calderas (Fig. 2.1; Lipman, 1984). The western margin of the Latir field is defined by the Rio Grande Rift valley (Meyer, 1991). Structural reconstruction combined with geochronology of volcanic rocks indicates that rifting began in the Latir field at 28 Ma, reached a maximum extensional rate between 26-25 Ma, and continued into the Miocene with rates slowing considerably (Meyer, 1991; Smith et al., 2002). Modern rifting began at approximately 15 Ma, and resulted in a few km of relief along the main Rio Grande Rift escarpment (Chapin, 1979; Tweto, 1979), exposing the potential plutonic roots of the volcanic rocks (Lipman, 1984).

Volcanism in the Latir field began approximately at the same time as rifting (Meyer and Foland 1991; Zimmerer, 2008). Volcanism is categorized into three phases: precaldera, ignimbrite, and postcaldera stages, correlating respectively to the waxing, ignimbrite, and waning stages defined by Lipman (2007). Precaldera volcanic rocks are dominated by intermediate compositions, but range from basalt to rhyolite (Lipman et al.,

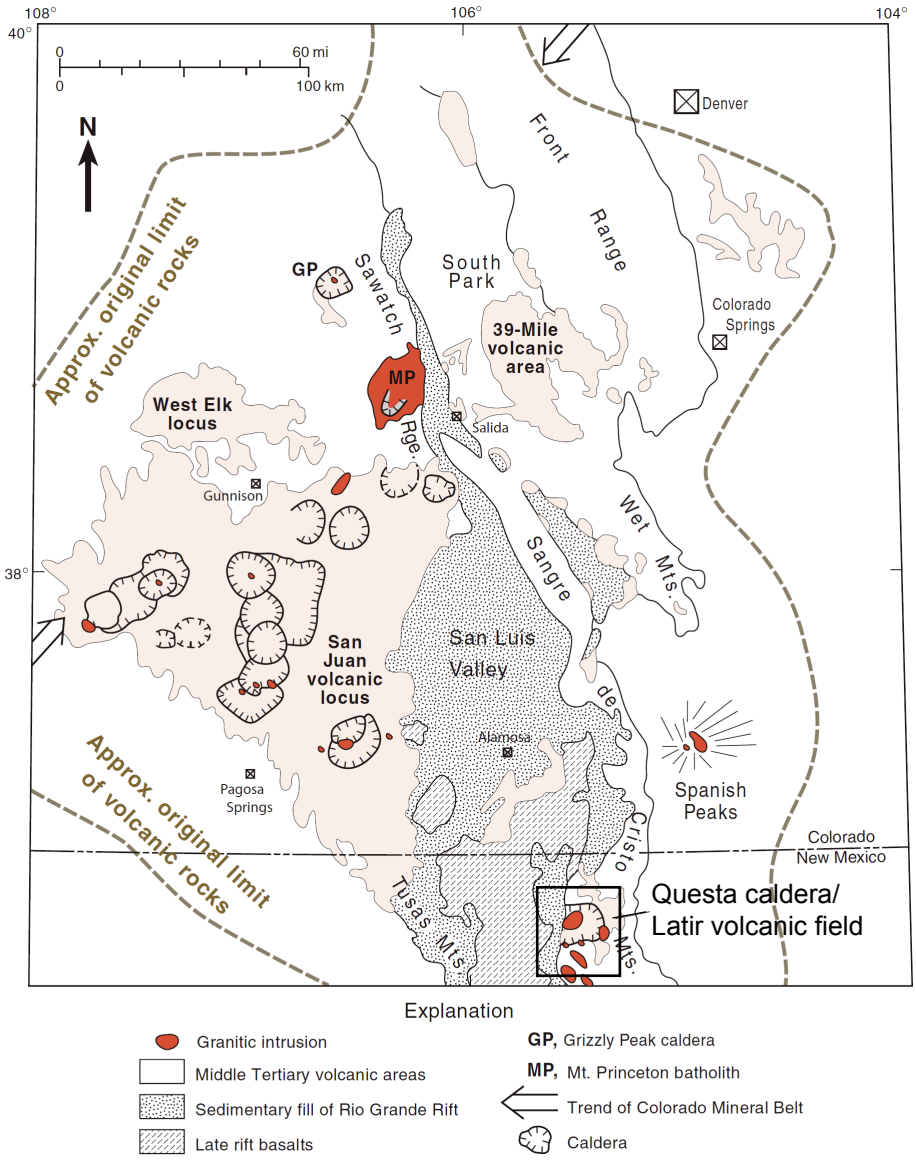


**Fig. 2.1**: Geologic map showing calderas in the Southern Rocky Mountain volcanic field modified from Lipman (2007) and originally from McIntosh and Chapin (2004). The focus of this study, the Questa caldera/Latir volcanic field is located in the southernmost portion of this map. A more detailed map of the Latir field is shown in figure 2.2.

1986). Recent detailed geochronology and geochemistry work reveals precaldera volcanic rocks fluctuate between alkaline and calc-alkaline compositions prior to ignimbrite eruption (Zimmerer, 2008), contrasting previous interpretations that precaldera volcanism evolved from calc-alkaline to alkaline then culminated with the peralkaline ignimbrite eruption (Lipman, 1984; Lipman et al., 1986). Latir volcanism initiated with the eruption of an alkalic andesite at 28.31 ± 0.19 Ma and the precaldera stage concluded with a rhyolite eruption at 25.27 ± 0.06 Ma (Zimmerer, 2008). Volcanism climaxed at 25.23 ± 0.05 Ma with the ignimbrite eruption of the ~500 $km^3$ peralkaline Amalia Tuff, a crystal-poor high-silica rhyolite welded tuff (Zimmerer, 2008). Postcaldera volcanism was dominated by intermediate composition volcanic eruptions; however, whereas precaldera and ignimbrite volcanic rocks are preserved as individual units, the only preserved postcaldera volcanic rocks are found as reworked deposits in sedimentary layers on two intrarift horst blocks (Thompson et al., 1986).

Nine subvolcanic plutons crop out within the Latir field (Fig. 2.2; Lipman, 1984). Existing geochronologic data suggest that the intrusive rock record is dominated by postcaldera rocks (Lipman et al., 1986, Czamanske et al., 1990; Zimmerer, 2008). These can be divided into three groups based on ages and spatial proximity (Lipman et al., 1986; Meyer, 1991). The Cañada Pinabete, Virgin Canyon, Rito del Medio, and Cabresto Lake plutons form the oldest intracaldera northern group. The Bear Canyon, Sulfur Gulch, and Red River plutons form the intermediate age caldera margin group. The Rio Hondo and Lucero Peak plutons form the youngest southern group. Early $^{40}Ar/^{39}Ar$ (Czamanske et al., 1990), K/Ar, and fission-track dates (Lipman et al., 1986), that were used to estimate the timing of intrusions were recently supplanted by detailed $^{40}Ar/^{39}Ar$

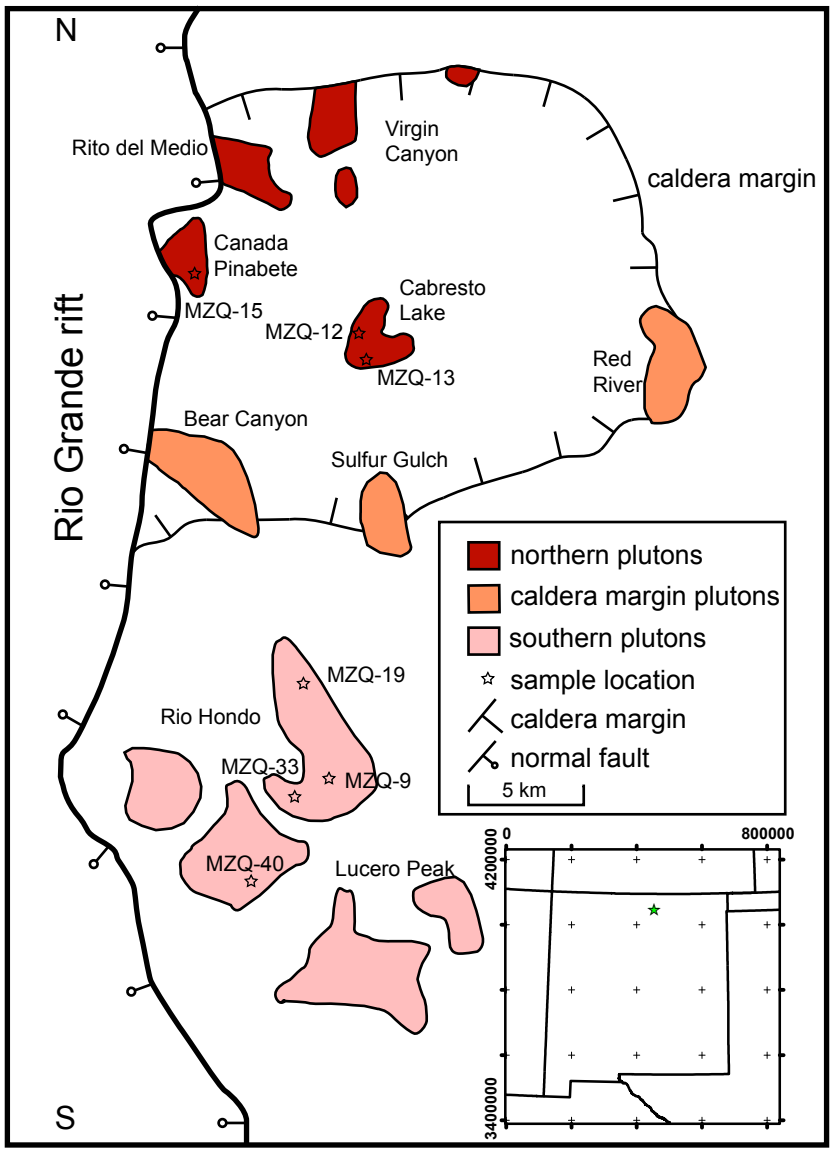


**Fig. 2.2**: Schematic illustration of plutons exposed within the Latir volcanic field, and approximate locations of samples analyzed for this study. Plutons categorized into three groups: northern (red), caldera margin (peach), and southern (pink).

thermochronology on hornblende, biotite and K-feldspar for all the intrusive rocks (Zimmerer, 2008); thus Zimmerer (2008) dates are preferred in this study (Table 2.1).

The northern pluton group includes the oldest exposed Latir intrusions that are interpreted to have formed contemporaneously with the caldera (Lipman et al., 1986). Within this group, the Cañada Pinabete and Virgin Canyon plutons are interpreted to be the oldest intrusions and, because they are similar petrographically and geochemically they are typically viewed as the same intrusion (Lipman et al., 1986; Johnson et al., 1989; Czamanske et al., 1990; Zimmerer, 2008).

Lipman (1988) identified three phases that comprise the Cañada Pinabete and Virgin Canyon plutons. The structurally highest phase, locally distinctive peralkaline granite, is interpreted to represent unerupted Amalia Tuff (Lipman et al., 1986; Johnson et al., 1989; Zimmerer, 2008). The other two phases, both metaluminous granites, are categorized as early and late components with the early phase being structurally above the late phase (Lipman, 1988). Paleomagnetic and petrologic evidence suggest that the plutons crystallized from the top down (Hagstrum and Lipman, 1986; Johnson et al., 1986). Lipman (1988) described the contact between the peralkaline and early metaluminous phase as "locally sharp but partly gradational" and suggests it results from incomplete mixing or a disturbed differential gradient. The three phases are roughly equally distributed in the Virgin Canyon pluton, but exposure of the Cañada Pinabete pluton is dominated by the late metaluminous granite. Argon geochronology of the phases yield complicated results. Zimmerer (2008) prefers plateau ages (26.50-25.28 Ma) that suggests the plutons may have formed prior to the Amalia Tuff (25.23 Ma;

Table 2.1 – $^{40}Ar/^{39}Ar$ Thermochronology of Latir Intrusions (Zimmerer, 2008)

| Unit | Sample | Material | Age (Ma) |
|---|---|---|---|
| **Southern plutons** | | | |
| Lucero Peak | MZQ-21 | biotite† | 19.22±0.10 |
| | | K-feldspar§ | 18.59±0.11 |
| | MZQ-32 | biotite† | 19.02±0.10 |
| | | K-feldspar§ | 19.27±0..09 |
| Rio Hondo | MZQ-9 | biotite† | 21.08±0.10 |
| | | K-feldspar§ | 21.73±0.12 |
| | MZQ-19 | biotite§ | 21.37±0.09 |
| | | K-feldspar† | 21.27±0.08 |
| | MZQ-33 | K-feldspar§ | 21.96±0.13 |
| **Caldera margin plutons** | | | |
| Bear Canyon | MZQ-8 | biotite† | 24.38±0.12 |
| | | K-feldspar† | 23.56±0.18 |
| | MZQ-34 | biotite† | 24.22±0.10 |
| | | K-feldspar† | 22.21±0.11 |
| Sulfur Gulch | MZQ-6 | biotite† | 24.57±0.14 |
| | | K-feldspar† | 26.50±0.12 |
| | AR-171 | biotite† | 24.48±0.10 |
| Red River | MZQ-5 | biotite† | 24.78±0.06 |
| | | K-feldspar§ | 24.36±0.21 |
| **Northern plutons** | | | |
| Cabresto Lake | MZQ-12 | biotite† | 24.65±0.13 |
| | | K-feldspar‡ | 24.68±0.09 |
| | MZQ-13 | biotite† | 24.68±0.11 |
| | | K-feldspar† | 25.51±0.33 |
| Rito del Medio | MZQ-16 | biotite† | 25.03±0.05 |
| | | K-feldspar† | 25.06±0.15 |
| | MZQ-39 | biotite† | 24.66±0.17 |
| | | K-feldspar† | 24.65±0.08 |
| Cañada Pinabete | MZQ-15 | biotite† | 25.28±0.09 |
| | | K-feldspar§ | 29.19±0.27 |
| Virgin Canyon | MZQ-1 | K-feldspar§ | 29.53±0.24 |
| | MZQ-2 | K-feldspar† | 26.50±0.09 |
| | MZQ-38 | K-feldspar† | 25.78±0.07 |

Preferred dates reported by Zimmerer (2008).
† Dates calculated from plateau.
‡ Dates calculated from inverse isochron.
§ Dates calculated from the total gas released during analysis.

Zimmerer, 2008) however, inverse isochron ages for the same samples yield mostly younger dates (25.6-25.2 Ma) and are all within uncertainty of the Amalia Tuff.

Following intrusion of the northern plutons, magmatism shifted toward the southern margin of the caldera (Lipman et al., 1986; Czamanske et al., 1990; Zimmerer, 2008). Field relations show the caldera margin plutons cutting through the Amalia Tuff, confining the age of emplacement to occur after ignimbrite eruption (Meyer and Foland, 1991), and confirmed by $^{40}Ar/^{39}Ar$ thermochronology on biotite (24.78-22.22 Ma; Zimmerer, 2008). The group consists of three intrusive rock map units: The Bear Canyon and Sulfur Gulch plutons, and the Red River intrusive complex. The Bear Canyon and Sulfur Gulch plutons are hydrothermally altered high-silica granites, containing zones of molybdenite ore. Drilling associated with molybdenum mining suggests that these plutons may be connected several hundred meters below the surface (Leonardson et al., 1983). The Red River intrusive complex, exposed on the southeast edge of the caldera margin, is a mostly moderate to high-silica (68-78 wt% $SiO_2$) suite dominated by numerous dikes of various compositions (Johnson et al., 1989).

The Rio Hondo pluton, of the southern pluton group, is the largest exposed intrusive rock map unit in the Latir field and varies compositionally from equigranular granite to megacrystic K-feldspar granodiorite. The granitic unit is thought to represent the cap or roof of a magma chamber, formed by differentiation from the main granodiorite body (Lipman et al., 1986; Johnson et al., 1989). The Rio Hondo pluton is intruded by hundreds of granitic dikes not present in the Lucero Peak pluton, the other southern pluton group member (Lipman and Reed, 1989). Argon thermochronology indicates that both the Rio Hondo pluton (21.37-21.08 Ma) and the Lucero Peak pluton

(19.22-19.02 Ma), formed significantly after the ignimbrite eruption (Zimmerer, 2008), making the Lucero Peak pluton the youngest and southern-most exposed intrusion in the Latir field.

Early K/Ar and fission track thermochronology was used to frame the geochemical evolution of the Latir plutonic and volcanic rocks (Dillett and Czamanske, 1987; Johnson and Lipman, 1988; Lipman, 1988; Johnson et al., 1989; Johnson et al., 1990). Using major, trace, and rare earth elements (REE) Johnson et al. (1988; 1989) concluded that the extrusive and intrusive rocks were each highly evolved and suggested that, whereas both suites can be generated by magma chamber fractionation, the process differs for plutonic and volcanic rocks. These authors proposed that volcanic rocks evolved in crystal-poor magma chambers in which crystallization primarily involved major minerals (e.g. alkali feldspar, plagioclase, quartz) yielding relatively enriched concentrations of REE and trace elements. In contrast they proposed that the plutonic rocks evolved in crystal-rich chambers with extensive accessory mineral fractionation (e.g. titanite, apatite, zircon) resulting in low concentrations of trace elements, specifically middle REE.

Johnson et al. (1989) proposed the compositional variations found within the Cañada Pinabete, Virgin Canyon, and Rio Hondo plutons to result from crystal fractionation, similar to the process envisioned to generate ignimbrites in the pluton-building caldera model. If the compositional variations are generated by crystal fractionation, formation of these compositional phases would be approximately concurrent with the stratigraphically highest and most evolved melts crystallizing last,

and the chemical relationship between phases should display complementary chemical compositions.

# 3. METHODS

One sample of the Cañada Pinabete pluton, two samples of the Cabresto Lake pluton, and four samples from the Rio Hondo pluton were collected for zircon U/Pb geochronology. The samples are the same as those used by Zimmerer (2008) for $^{40}Ar/^{39}Ar$ thermochronology. All samples were crushed using a jaw crusher and a disc mill. Zircon was isolated using standard density (water table and heavy liquids) and magnetic separation techniques. Individual grains were selected using a binocular microscope on the basis of size, clarity, and morphology. The selected grains were thermally annealed for 48 hours at 900°C (Mattinson, 2005) and chemically abraded for 12 hours at 220°C in an attempt to remove any domains that experienced Pb loss (procedure modified from Mundil et al., 2004). Zircons were separated into fractions, dissolved in 29 M HF acid and spiked using a $^{205}Pb$-$^{233}U$-$^{236}U$ tracer (Krogh, 1973; Parrish and Krogh, 1987). Anion exchange column chromatography was used to isolate U and Pb from the dissolved solution. Analysis of U and Pb was completed using a VG Sector 54 thermal ionization mass spectrometer (TIMS) at the University of North Carolina at Chapel Hill. Uranium was run as a metal after loading in graphite and $H_3PO_4$ on single Re filaments. Lead was loaded in silica gel on single Re filaments. Both U and Pb were analyzed in single-collector peak-hopping mode using the Daly ion-counting system. Data reduction was completed using Tripoli™ software and percent standard errors are reported at 2σ confidence. Data processing and age calculations were completed with the PbMacDat-2 program by D.S. Coleman using the algorithms of

Ludwig (1989, 1990) and *Isoplot* v. 3.00 (Ludwig, 2003). Decay constants used are $^{238}U=1.55125 \times 10^{-10}\ a^{-1}$ and $^{235}U=9.8485 \times 10^{-10}\ a^{-1}$ (Steiger and Jäger, 1977).

Initially samples consistently produced poor results with apparent erroneously high common Pb concentrations and poor radiogenic Pb yield, so modifications were made to the dissolution and column procedures in an attempt to improve results. After conducting experiments to isolate potential problems two issues were identified and modifications made to the procedures. One effective modification was altering the dissolution process from using HF gas to using HF liquid. Using HF gas likely caused precipitation of an insoluble fluoride salt, which resulted in only a fraction of the total U and Pb (sample + tracer) being isolated during column chemistry, thus leading to poor Pb yield. Since only a fraction of the total tracer was loaded onto the filament, the loading blank was exaggerated, and total common Pb artificially appeared high.

A second successful modification was changing the anion column chemistry procedure. Initially 50 uL columns were used, but column length and geometry varied creating inconsistencies between columns. New uniformly shaped 150 uL columns were cleaned and calibrated, resulting in superior results with far greater consistency during analysis. Consistency of successful analyses was greatly enhanced after these two procedural modifications were adopted.

# 4. RESULTS

Data are presented in Table 4.1. Zircons from all samples contain few inclusions and lack apparent inherited cores or rims. For most samples there is scatter in ages beyond analytical uncertainty, but there is also a cluster of a subset of analyses defined as three or more overlapping data points. For these samples both the range in $^{206}Pb/^{238}U$ ages and the concordia age of the cluster is reported.

## 4.1 Cañada Pinabete pluton

One sample (MZQ-15) of the late metaluminous phase of the Cañada Pinabete pluton was analyzed (Fig. 4.1-G). Three concordant and one slightly normally discordant fraction of MZQ-15 span from 25.41-25.17 Ma and three concordant points cluster and yield an age of 25.23 ± 0.09 Ma (MSWD = 1.8). Two samples of the peralkaline phase were processed, but no zircon was liberated during initial separation steps. Scanning electron microscopy revealed that the traces of zircon contained within the peralkaline phase are amorphous and of questionable use in determining the crystallization age of the sample.

## 4.2 Cabresto Lake pluton

Two spatially and mineralogically distinct samples (MZQ-12 and MZQ-13) of the Cabresto Lake pluton were dated. The two samples are compositionally similar although only MZQ-13 contains titanite.

Results for the two samples yield overlapping ages at approximately 25 Ma (Fig. 4.1-E,F,I). Four concordant fractions of MZQ-12 cluster and yield an age of 25.02 ± 0.05 Ma (MSWD = 1.2). Five concordant fractions of MZQ-13 cluster and yield an age of 24.94 ± 0.05 Ma (MSWD = 0.5).

## 4.3 Rio Hondo pluton

Four spatially and compositionally distinct samples (MZQ-9, MZQ-19, MZQ-33, and MZQ-40) of the Rio Hondo pluton were analyzed. The structurally highest sample (MZQ-33) was collected from near the interpreted roof of the Rio Hondo (Lipman, 1988; Czmanske et al., 1990), and is high-silica granite with abundant rapikivi K-feldspar megacrysts. Samples MZQ-19, MZQ-9, and MZQ-40 are granodiorite with the latter two hosting rapakivi K-feldspar megacrysts. The relative structural positioning of the granodiorite samples is difficult to assess because differential uplift and faulting results in deeper level exposure in the southern region of the pluton (Lipman, 1988).

Rio Hondo zircons yield ages from 23.00-22.47 Ma and each sample yields a concordant ellipse that does not overlap with the other samples of the Rio Hondo pluton within uncertainty (Fig. 4.1- A-D, H). Five concordant and one normally discordant fraction of MZQ-33 span from 23.00-22.77 Ma and three points cluster and yield an age of 22.99 ± 0.12 Ma (MSWD = 2.6). Four concordant fractions of MZQ-40 span from 22.84-22.71 Ma and three points cluster and yield an age of 22.81 ± 0.06 Ma (MSWD = 1.9). Five concordant fractions of MZQ-19 cluster and yield an age of 22.63 ± 0.03 Ma (MSWD = 1.0). Four concordant fractions of MZQ-9 span from 22.62-22.47 Ma and three points cluster and yield an age of 22.49 ± 0.04 Ma (MSWD = 0.7).

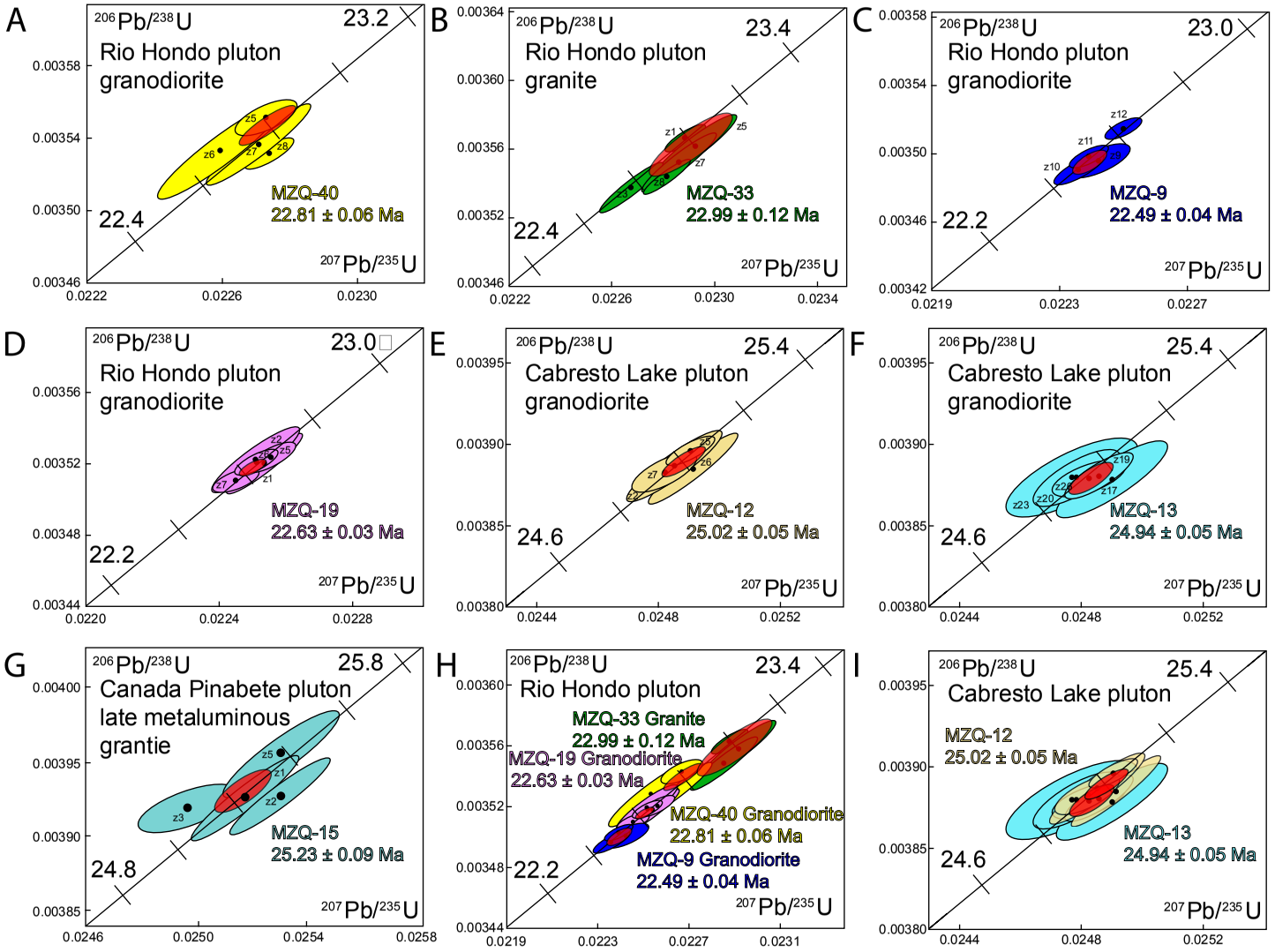


**Fig. 4.1**: Conventional U/Pb concordia diagrams for zircons analyzed in this study for individual samples of the Rio Hondo (A-D), Cabresto Lake (E,F), and Canada Pinabete (G) plutons. H) Concordia diagram displaying all the Rio Hondo pluton samples. I) Concordia diagram displaying the Cabresto Lake pluton samples. Ages reported are weighted mean 206Pb/238U age for a cluster (red ellipses) of three or more points and are known to the 2-sigma confidence level. Data processing and age calculations were completed using software PbMacDat-2 by D.S. Coleman using the algorithms of Ludwig (1989, 1990) and concordia diagrams were constructed using Isoplot v. 3.00 (Ludwig, 2003).

TABLE 4.1 - ZIRCON U/Pb GEOCHRONOLOGY

| | | conc. (ppm) | | 206 Pb† | 206 Pb‡ | error | 207 Pb‡ | error | 207 Pb‡ | error | ages (Ma) 206 Pb | 207 Pb | 207 Pb | corr. | total common |
|---|---|---|---|---|---|---|---|---|---|---|---|---|---|---|---|
| fract.(n) | wt. (mg) | U | Pb* | 204 Pb | 238 U | % | 235 U | % | 206 Pb | % | 238 U | 235 U | 206 Pb | coef. | Pb (pg) |
| **MZQ-15** Metaluminous Canada Pinabete (0450662, 4068102) | | | | | | | | | | | | | | | |
| Z1 (3) | 0.028 | 375.1 | 1.60 | 1047.6 | 0.003921 | 0.38 | 0.02516 | 0.47 | 0.04655 | 0.27 | 25.22 | 25.24 | 26.37 | 0.82 | 2.5 |
| Z2 (2) | 0.0315 | 355.6 | 1.55 | 963.6 | 0.003922 | 0.42 | 0.02529 | 0.50 | 0.04678 | 0.26 | 25.23 | 25.36 | 37.75 | 0.85 | 3.0 |
| Z3 (3) | 0.0287 | 652.2 | 2.80 | 1839.9 | 0.003913 | 0.25 | 0.02496 | 0.65 | 0.04627 | 0.57 | 25.17 | 25.04 | 11.74 | 0.49 | 2.6 |
| Z5 (5) | 0.0259 | 392.1 | 1.73 | 1118.2 | 0.003950 | 0.36 | 0.02530 | 0.53 | 0.04645 | 0.37 | 25.41 | 25.37 | 21.09 | 0.72 | 2.3 |
| **MZQ-12** Granite of Cabresto Lake (04055802, 4066000) | | | | | | | | | | | | | | | |
| Z2 (3) | 0.0354 | 581.3 | 2.68 | 977.5 | 0.003883 | 0.57 | 0.02490 | 0.62 | 0.04652 | 0.25 | 24.98 | 24.98 | 24.54 | 0.92 | 5.3 |
| Z5 (4) | 0.0345 | 505.8 | 2.27 | 1970.7 | 0.003892 | 0.24 | 0.02495 | 0.33 | 0.04651 | 0.22 | 25.04 | 25.03 | 24.00 | 0.75 | 2.2 |
| Z6 (4) | 0.0325 | 644.8 | 2.90 | 1374.4 | 0.003881 | 0.56 | 0.02496 | 0.60 | 0.04665 | 0.20 | 24.97 | 25.04 | 31.53 | 0.94 | 3.8 |
| Z7 (3) | 0.0330 | 486.7 | 2.09 | 1336.7 | 0.003879 | 0.31 | 0.02487 | 0.45 | 0.04651 | 0.31 | 24.96 | 24.95 | 23.93 | 0.72 | 3.0 |
| **MZQ-13** Granite of Cabresto Lake (04054977, 4065797) | | | | | | | | | | | | | | | |
| Z17 (2) | 0.0229 | 422.9 | 1.88 | 647.4 | 0.003874 | 0.60 | 0.02495 | 0.72 | 0.04671 | 0.38 | 24.93 | 25.02 | 34.41 | 0.85 | 3.8 |
| Z19 (3) | 0.0206 | 716.8 | 3.16 | 1076.2 | 0.003876 | 0.37 | 0.02491 | 0.45 | 0.04660 | 0.25 | 24.94 | 24.98 | 29.02 | 0.83 | 3.4 |
| Z20 (2) | 0.0233 | 535.9 | 2.29 | 904.6 | 0.003876 | 0.44 | 0.02483 | 0.59 | 0.04647 | 0.38 | 24.94 | 24.91 | 22.32 | 0.76 | 3.5 |
| Z23 (3) | 0.0176 | 431.0 | 1.91 | 632.7 | 0.003875 | 0.62 | 0.02482 | 0.89 | 0.04645 | 0.60 | 24.93 | 24.89 | 20.94 | 0.73 | 3.0 |
| Z26 (3) | 0.0296 | 429.1 | 1.84 | 1383.3 | 0.003875 | 0.30 | 0.02488 | 0.48 | 0.04656 | 0.36 | 24.93 | 24.95 | 26.59 | 0.65 | 2.3 |
| **MZQ-9** Megacrystic Granodiortie of Rio Hondo (0455754, 4051203) | | | | | | | | | | | | | | | |
| Z9 (3) | 0.0259 | 501.7 | 1.97 | 1487.1 | 0.003497 | 0.29 | 0.02245 | 0.43 | 0.04656 | 0.31 | 22.50 | 22.54 | 26.49 | 0.69 | 2.0 |
| Z10 (4) | 0.0256 | 818.8 | 3.15 | 1807.7 | 0.003492 | 0.27 | 0.02238 | 0.35 | 0.04649 | 0.22 | 22.47 | 22.48 | 23.15 | 0.79 | 2.6 |
| Z11 (4) | 0.0207 | 1125.8 | 4.27 | 2583.6 | 0.003500 | 0.19 | 0.02242 | 0.27 | 0.04646 | 0.18 | 22.52 | 22.51 | 21.31 | 0.73 | 2.0 |
| Z12 (3) | 0.0339 | 681.2 | 2.61 | 2656.2 | 0.003516 | 0.18 | 0.02252 | 0.26 | 0.04646 | 0.18 | 22.62 | 22.62 | 21.77 | 0.71 | 2.0 |
| **MZQ-19** Megacrystic Granodiortie of Rio Hondo (0453613, 4055209) | | | | | | | | | | | | | | | |
| Z1 (2) | 0.0249 | 1132.3 | 4.65 | 1384.9 | 0.003518 | 0.47 | 0.02256 | 0.51 | 0.04652 | 0.19 | 22.64 | 22.66 | 24.67 | 0.93 | 4.6 |
| Z2 (2) | 0.0240 | 1013.5 | 4.07 | 1076.3 | 0.003520 | 0.53 | 0.02254 | 0.59 | 0.04643 | 0.25 | 22.65 | 22.63 | 20.24 | 0.90 | 5.2 |

| | | | | | | | | | | | | | | | |
|---|---|---|---|---|---|---|---|---|---|---|---|---|---|---|---|
| Z5 (2) | 0.0222 | 1082.2 | 4.12 | 1910.8 | 0.003521 | 0.24 | 0.02258 | 0.32 | 0.04651 | 0.21 | 22.66 | 22.68 | 24.29 | 0.75 | 2.8 |
| Z6 (2) | 0.0262 | 1076.5 | 4.25 | 2363.7 | 0.003519 | 0.21 | 0.02254 | 0.29 | 0.04646 | 0.19 | 22.64 | 22.63 | 21.62 | 0.75 | 2.7 |
| Z7 (3) | 0.0286 | 889.5 | 3.40 | 2858.6 | 0.003508 | 0.20 | 0.02248 | 0.31 | 0.04647 | 0.23 | 22.58 | 22.57 | 21.93 | 0.67 | 2.0 |
| **MZQ-33** Granite of Rio Hondo (0453636, 4039302) | | | | | | | | | | | | | | | |
| Z1 (2) | 0.0335 | 1684.2 | 6.33 | 2354.8 | 0.003574 | 0.28 | 0.02290 | 0.35 | 0.04647 | 0.20 | 23.00 | 22.99 | 22.23 | 0.82 | 5.5 |
| Z3 (2) | 0.0242 | 1028.8 | 3.90 | 1177.0 | 0.003538 | 0.52 | 0.02269 | 0.56 | 0.04652 | 0.19 | 22.77 | 22.78 | 24.52 | 0.94 | 4.8 |
| Z5 (3) | 0.0214 | 910.1 | 3.46 | 1420.9 | 0.003568 | 0.65 | 0.02294 | 0.70 | 0.04663 | 0.26 | 22.96 | 23.03 | 30.29 | 0.93 | 3.2 |
| Z7 (3) | 0.0271 | 766.0 | 2.87 | 1132.6 | 0.003556 | 0.60 | 0.02288 | 0.65 | 0.04665 | 0.22 | 22.88 | 22.97 | 31.51 | 0.94 | 4.2 |
| Z8 (3) | 0.0264 | 1352.0 | 5.26 | 1390.3 | 0.003546 | 0.36 | 0.02283 | 0.40 | 0.04669 | 0.16 | 22.82 | 22.92 | 33.56 | 0.91 | 5.9 |
| **MZQ-40** Megacrystic Granodiorite of Rio Hondo (0452777, 4046272) | | | | | | | | | | | | | | | |
| Z5 (3) | 0.0233 | 952.1 | 3.63 | 1653.7 | 0.003549 | 0.58 | 0.02269 | 0.65 | 0.04637 | 0.30 | 22.84 | 22.78 | 16.79 | 0.89 | 3.1 |
| Z6 (2) | 0.031 | 707.8 | 2.71 | 1149.4 | 0.003531 | 0.58 | 0.02256 | 0.65 | 0.04634 | 0.29 | 22.72 | 22.65 | 15.34 | 0.89 | 4.4 |
| Z7 (1) | 0.0154 | 1714.2 | 6.50 | 1490.2 | 0.003535 | 0.48 | 0.02267 | 0.54 | 0.04652 | 0.22 | 22.75 | 22.77 | 24.90 | 0.91 | 4.0 |
| Z8 (3) | 0.0242 | 1145.5 | 4.42 | 1737.4 | 0.003530 | 0.47 | 0.02270 | 0.51 | 0.04665 | 0.20 | 22.71 | 22.79 | 31.35 | 0.92 | 3.6 |



[*] Radiogenic Pb

[†] Measured ratio corrected for fractionation only. All Pb isotope ratios were measured using the Daly detector, and are corrected for mass fractionation using 0.15%/a.m.u.

[‡] Corrected for factionation, spike, blank, and initial common Pb. After subtraction of blank Pb (<3.0 pg), common Pb corrections were unnecessary for most fractions. For fractions with total common Pb in excess of 3.0 pg, corrections were made using Stacey and Kramers (1975) initial Pb.

[**] All locations reported as UTM zone 13N coordinates using NAD 27.

Analysis accomplished with a VG Sector 54 thermal ionization mass spectrometer at the University of North Carolina. Decay constants used are $^{238}U$ = 0.155125 x 10-9 a-1, and $^{235}U$ = 0.98485 x 10-9 a-1 (Steiger and Jäger, 1977). Weights are estimated using a video camera and scale, and are known to within 10%. Data reduction and error analysis was accomplished using PbMacDat-2 by D.S. Coleman, using the algorithms of Ludwig (1989, 1990) and all errors are reported in percent at the 2σ confidence interval.

# 5. DISCUSSION

## 5.1 Intrusive history of the Cañada Pinabete, Cabresto Lake, and Rio Hondo plutons

Seven new high-resolution U/Pb zircon ages presented in this study establish an intrusive history for the Cañada Pinabete, Cabresto Lake, and Rio Hondo plutons. One sample of the late metaluminous phase of the Cañada Pinabete pluton yields an age of 25.23 ± 0.09 Ma, similar to both the age estimate using fission track and K/Ar (26 Ma) by Lipman et al. (1986), and $^{40}Ar/^{39}Ar$ plateau age (24.7 Ma) reported by Czamanske et al. (1990). Two Cabresto Lake pluton samples yield statistically indistinguishable ages from one another of 25.02 ± 0.05 to 24.94 ± 0.05 Ma, confirming the ages reported in previous work (Lipman et al., 1986; Czamanske et al., 1990; Zimmerer, 2008). Four Rio Hondo pluton samples range in age from 22.99 ± 0.12 to 22.49 ± 0.04 Ma. This age range is substantially younger than the age estimate of 25-26 Ma from fission track and $^{40}K/^{39}Ar$ methods reported by Lipman et al. (1986), but is somewhat older than $^{40}Ar/^{39}Ar$ ages (Table 2.1) reported by Czamanske et al. (1990) and Zimmerer (2008).

The ages determined in this study support previous interpretations of magmatism beginning with the northern plutons and migrating south (Lipman et al., 1986; Czamanske et al., 1990). The zircon U/Pb age of the late metaluminous Cañada Pinabete pluton (25.23 ± 0.09 Ma) is identical to the sanidine $^{40}Ar/^{39}Ar$ age reported for the Amalia Tuff (25.23 ± 0.05 Ma; Zimmerer, 2008), using the decay constant of Steiger and

Jäger (1977). The post-caldera Cabresto Lake pluton formed ~200 K.y. after ignimbrite eruption and two samples yield overlapping ages suggesting that the unit was assembled rapidly. The Rio Hondo pluton formed ~2 M.y. after ignimbrite eruption and the time between formation of the Cabresto Lake and Rio Hondo plutons spans the majority of post-caldera magmatic activity. The Rio Hondo pluton formed over at least 500 k.y. indicating protracted pluton assembly. Thus, the ages demonstrate that the pluton that formed soon after caldera eruption, presumably during peak magma input, assembled rapidly and the pluton that formed after peak magma input was likely assembled incrementally, thereby supporting the general caldera evolution model proposed by Lipman (2007).

The span of zircon U/Pb ages for the Rio Hondo pluton is not uncommon in large intrusive rock map units. In a variety of tectonic settings, zircon U/Pb geochronology yields ages that range from 0.09 to 4 M.y. between multiple samples from individual plutons (Coleman et al., 2004; Cruden et al., 2005; Matzel et al., 2006; Gracely, 2007; Michel et al., 2008). Those studies attribute these age ranges to incremental intrusion, in which mapped plutons are the final products of multiple pulses of magma that intruded the upper crust. During incremental assembly, early pulses cool rapidly and quickly reach the solidus temperature after intrusion. As the local geothermal gradient is elevated by continued intrusion, later pulses cool more slowly allowing the possibility for formation of a steady-state magma chamber that is smaller than the total assembled body (Hanson and Glazner, 1995; Wiebe and Collins, 1998; Yoshinobu et al., 1998). Consequently, voluminous eruptions are unlikely to be related to incrementally

assembled plutons, because there never is a large volume of magma generated for eruption.

## 5.2 Pluton filling rates

The well-determined geochronology and structural relief make the Rio Hondo pluton an interesting case study for examining pluton filling rates. The geochronology presented in this study shows that the pluton took at least 500,000 years to form. Structural relief and field observations provide a minimum pluton thickness, used to calculate pluton volume. The roof of the pluton is exposed at low-angle contacts between plutonic and basement rocks along ridge crests (Lipman, 1988). At low elevations, the Rio Hondo pluton contains high concentrations of mafic enclaves, interpreted in other intrusions to result from underplated mafic dikes (Wiebe et al., 1997; Bachl et al., 2001), suggesting a level near the pluton floor. These observations yield a thickness estimate of 1.2 km for the Rio Hondo pluton. Because the pluton floor is not exposed the volume estimate is a minimum. However, the oblate geometry of the Rio Hondo pluton implied by the minimum outcrop area (90 $km^2$) and a 1.2 km thickness provides an aspect ratio of 7.5:1, comparable to most other pluton aspect ratios (Cruden and McCaffrey, 2001; Bachmann and Bergantz, 2008a). This aspect ratio also seems reasonable when considering that plutons emplaced in extensional regimes have a relatively modest thickness in comparison to plutons emplaced in other tectonic settings (Vigneresse, 1995; Cruden, 2006).

Using the 1.2 km thickness and a filling time of 0.5 M.y., the Rio Hondo pluton yields a steady-state filling rate of 6.1 x $10^{-3}$ $m^3/s$. If the thickness is underestimated, the filling rate is also undervalued. Assuming a maximum thickness of 2.2 km for the Rio

Hondo pluton, calculated using assumptions for "typical" plutons by Petford et al. (2000), yields an aspect ratio of 4.1:1 and a filling rate of 1.1 x $10^{-2}$ $m^3/s$. Estimated filling rates for other plutons with precise geochronologic control yield rates similar to that of the Rio Hondo pluton (Table 5.1) ranging from 4.8 x $10^{-3}$ $m^3/s$ to 4.2 x $10^{-2}$ $m^3/s$.

The filling rates for the Rio Hondo and the other plutons reviewed are significantly slower than the modeled rate of 1.0 $m^3/s$ (Petford et al., 2000), calculated from estimates for pluton volume, magma viscosities, wall-rock/magma density contrasts, and dike morphologies. The discrepancy between calculated and model filling rates is partially explained by noting that the modeled pluton thickness may be overestimated as Petford et al. (2000) acknowledge. However, the most significant discrepancy is likely to result from the pluton-building timescales. Petford et al. (2000) favor pluton-building timescales of <100,000 years and further suggest plutons may be completely emplaced in under 1,000 years, however these timescales are built on the assumption of continuous magma recharge. Because more recent work demonstrates numerous plutons preserve evidence for complex and periodic intrusive histories (e.g. Coleman et al., 2004; Cruden et al., 2005; Matzel et al., 2006; Gracely, 2007; Michel et al., 2008, this study) the assumption of continuous magma recharge appears to be flawed. Additionally, the range of ages for plutons must be interpreted as a minimum pluton building time, because additional sampling could yield ages outside of those reported, thus further decreasing estimates of pluton filling rates. Therefore, the pluton filling rates and subsequent pluton-building timescales suggested by Petford et al. (2000) are unlikely and may occur only in atypical situations.

TABLE 5.1 - PLUTON FILLING RATES

| Pluton | Surface area ($km^2$) | Thickness (km)[†] | Aspect ratio | Volume ($km^3$) | Building time (My)[‡] | Filling rate ($m^3/s$) |
|---|---|---|---|---|---|---|
| Rio Hondo | 80 | 1.2 | 7.5 | 96 | 0.5 | 0.006 |
| Torres del Paine | 96 | 1.25 | 7.8 | 120 | 0.09 | 0.042 |
| Half Dome | 300 | 10 | 1.7 | 3000 | 3.9 | 0.024 |
| Mt. Stuart | 480 | 2.5 | 8.8 | 1200 | 5.5 | 0.007 |
| Ten Peak | 197 | 2 | 7.0 | 394 | 2.6 | 0.005 |

[†]Thickness estimated from observations for Rio Hondo, Mt. Stuart, and Ten Peak plutons. Thickness estimated from geophysical studies for Torres del Paine (Skarmeta and Castelli, 1977), and Half Dome (Oliver, 1977).

[‡]Geochronology established for the Rio Hondo (this study), Torres del Paine by Michel et al. (2008), Half Dome by Coleman et al. (2004), Mt Stuart and Ten Peak by Matzel et al. (2006).

## 5.3 Integrating U/Pb and Ar/Ar geochronology

Multiple geochronometers with different closure temperatures can be used to establish the thermal history of an intrusive body (Dodson, 1973; McDougall and Harrison, 1989; Holm and Dakka, 1993). Calibration of U/Pb and Ar/Ar systems is challenging due to the difference of uncertainty in the decay constants (Ivanov, 2006; Krumrei et al. 2006; Matzel et al., 2006). Steiger and Jäger (1977) established the widely used decay constant values for $^{238}U$ ($\lambda$=1.551 ± 0.024 $e^{-10}yr^{-1}$), $^{235}U$ ($\lambda$=9.846 ± 0.048 e-$^{10}yr^{-1}$), and $^{40}K$ ($\lambda$=5.543 ± 0.020 $e^{-10}yr^{-1}$) with U decay constant errors reported by Jaffey et al. (1971) and K decay constant error reported by Min et al. (2000). Accurate calibration of chronometers is particularly important when investigating young rocks because the uncertainty in decay constants can exceed uncertainty in dates from analytical precision alone. The Fish Canyon Tuff, a widely used standard in $^{40}Ar/^{39}Ar$ geochronology, yields zircon ages ubiquitously older (0.4-0.5 Ma) than sanidine $^{40}Ar/^{39}Ar$ ages when using the Steiger and Jäger (1977) decay constants (Oberli et al., 1990; Bachmann et al., 2007b). This systematic difference was attributed to zircon residence in a long-lived magma chamber until Schmitz and Bowring (2001) established a $^{230}Th$ corrected disequilibrium U/Pb age on Fish Canyon Tuff titanite and concluded that prolonged residence was unlikely thus the $^{40}K$ decay constant was potentially undervalued.

Several studies have attempted to recalculate the $^{40}K$ decay constant (Audi et al., 1997; Min et al., 2000; Kossert and Gunther, 2004), and establish the precise $^{40}Ar/^{39}Ar$ age of standards including the Fish Canyon Tuff (Renne et al., 1998; Kuiper et al., 2008). The decay constant proposed by Min et al. (2000; $\lambda$=5.463 ± 0.214 $e^{-10}yr^{-1}$) demonstrates

that the uncertainty in the Steiger and Jäger (1977) $^{40}$K decay constant was under-assigned. The Min et al. (2000) decay constant was used by Kuiper et al. (2008) during calculations to determine the accurate age of the Fish Canyon Tuff. Kuiper et al. (2008) recognized that if astronomical age estimates could be determined for a sequence of sedimentary rocks intercalated with volcanic tephras, the $^{40}$Ar/$^{39}$Ar ages of the tephras must be consistent with the astronomical age estimates. Once this was established, the $^{40}$Ar/$^{39}$Ar ages of the tephras became the known variable so the samples were viewed as the standards, and the age of the actual standard, in this investigation the Fish Canyon Tuff, was recalculated. The age for the Fish Canyon Tuff proposed by Kuiper et al. (2008) increases the accepted age from 28.02 ± 0.56 Ma (Renne et al., 1998) to 28.201 ± 0.046 Ma closing most of the gap between U/Pb and $^{40}$Ar/$^{39}$Ar ages of the Fish Canyon Tuff. The new Fish Canyon Tuff age, combined with the Min et al. (2000) $^{40}$K decay constant, results in $^{40}$Ar/$^{39}$Ar dates increasing in age by approximately 0.65% relative to dates calculated using the Steiger and Jäger (1977) $^{40}$K decay constant and Renne et al. (1998) Fish Canyon Tuff age. Additional independent studies are necessary to confirm the finding of Kuiper et al. (2008) before the geochronology community accepts the new age of the Fish Canyon Tuff as the best current estimate. However, participants in the 2009 EARTHTIME meeting unanimously agreed to informally adopt the Kuiper et al. (2008) standard. Consequently this discussion focuses on $^{40}$Ar/$^{39}$Ar ages calculated using the $^{40}$K decay constant proposed by Min et al. (2000) with the standard proposed by Kuiper et al. (2008), but the implications of using the $^{40}$K decay constant proposed by Steiger and Jäger (1977) with the standard proposed by Renne et al. (1998) are also explored.

In order to understand the thermal evolution of plutons in the Latir field, cooling plots were constructed for samples from the Cabresto Lake and Rio Hondo plutons (Fig. 5.1). Because zircon separates were obtained from the identical samples that Zimmerer (2008) used when determining biotite and K-feldspar $^{40}Ar/^{39}Ar$ ages, there is no uncertainty introduced through comparison of data from different samples. Using geochemical data from Johnson et al. (1989), the zircon saturation temperature is calculated to be ~800°C for the Cabresto Lake pluton and ~725°C for the Rio Hondo pluton (Watson and Harrison, 1983; Miller et al., 2003). Biotite and K-feldspar closure temperatures are estimated to be approximately 300°C and 250°C, respectively (Harrison et al., 1985). Although the closure temperatures are only estimates, these temperatures provide a framework for understanding differences between cooling histories of multiple plutons.

For samples from which we have both biotite and K-feldspar $^{40}Ar/^{39}Ar$, calculation of cooling rates through biotite closure yield the same result within uncertainty as cooling rates through K-feldspar closure. Using the $^{40}K$ decay constant reported by Min et al. (2000) with the standard reported by Kuiper et al. (2008) the Cabresto Lake pluton samples (MZQ-12, MZQ-13) yield cooling rates of 2.4°C/K.y. and 5.0°C/K.y. respectively, indicating rapid cooling below the biotite closure temperature soon after intrusion. In contrast, all samples of the Rio Hondo pluton yield slow cooling rates. The northernmost granodiorite sample (MZQ-19) of the Rio Hondo pluton produces a monotonic cooling rate of 0.39°C/K.y. from zircon saturation temperature to K-feldspar closure temperature, whereas a megacystic K-feldspar granodiorite sample (MZQ-9) yields a monotonic cooling rate of 0.33°C/K.y. from zircon saturation to biotite

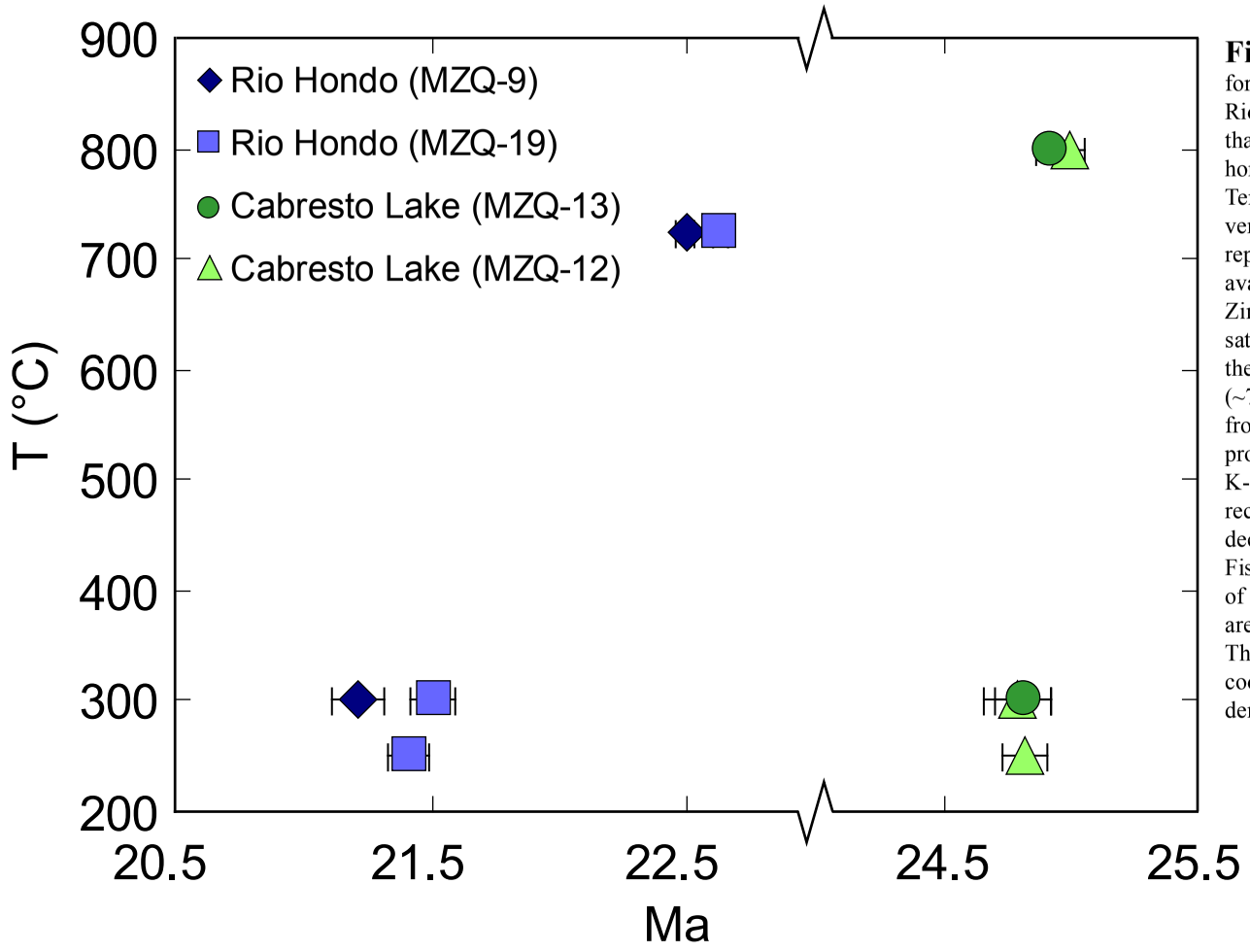


**Fig. 5.1**: Time/temperature cooling plots for the Cabresto Lake (green symbols) and Rio Hondo (blue symbols) plutons. Note that time progresses towards the left on the horizontal axis and is non-continuous. Temperature increases towards the top on the vertical axis. Different symbol types represent zircon, biotite, and K-feldspar (if available) ages from different samples. Zircon ages were determined in this study and saturation temperatures were calculated for the Cabresto Lake (~800°C) and Rio Hondo (~725°C) plutons using geochemical data from Johnson et al. (1989) and following the procedure of Miller et al. (2003). Biotite and K-feldspar dates from Zimmerer (2008) are recalculated using the Min et al. (2000) 40K decay constant and the Kuiper et al. (2008) Fish Canyon tuff age. Closure temperatures of 300°C for biotite and 250°C for K-feldspar are estimated from Harrison et al. (1985). The Cabresto Lake pluton displays rapid cooling whereas the Rio Hondo pluton demonstrates more protracted cooling.

closure temperatures. Using the $^{40}K$ decay constant proposed by Steiger and Jäger (1977) with the standard reported by Renne et al. (1988), all $^{40}Ar/^{39}Ar$ ages are younger, therefore cooling rates are slowed by approximately 50% for the Cabresto Lake samples and approximately 10% for Rio Hondo samples.

The disparity between cooling histories for the Cabresto Lake and Rio Hondo plutons is likely attributed to many factors. Exposure suggests the Cabresto Lake pluton is significantly smaller then the Rio Hondo pluton (Fig. 2.2), therefore the rate of heat loss by diffusion is expected to be greater for the Cabresto Lake pluton. Zircon U/Pb ages indicate the Cabresto Lake pluton assembled rapidly and soon after ignimbrite eruption. Magma input rates are likely to be greatest during ignimbrite formation (Lipman, 2007). Therefore, it seems reasonable that the Cabresto Lake pluton assembled rapidly after ignimbrite eruption and cooled immediately after intruding. In contrast, the much younger Rio Hondo pluton intruded during the waning stages of magmatism when magma input rates may have been sufficiently less. The zircon geochronology suggests that the Rio Hondo pluton was assembled over at least 500 k.y., and the addition of later magma pulses may have allowed the system to maintain temperatures in excess of the biotite and K-feldspar closure temperatures for extended time periods.

If the Cabresto Lake pluton cooled rapidly because of the depth of emplacement and formation during high magma input, then the Cañada Pinabete pluton would also be expected to cool rapidly given it likely formed at structurally higher levels and during the peak of magma input. Cooling rates were not calculated for the Cañada Pinabete pluton because the zircon U/Pb age (25.23 ± 0.09 Ma) is within uncertainty of the biotite Ar/Ar age (25.28 ± 0.08 Ma) reported by Zimmerer (2008) suggesting very rapid cooling.

## 5.4 Potential plutonic/volcanic rock pairs

The geochronology of the Cañada Pinabete pluton and Amalia Tuff highlight the importance of accurate calibration of chronometers when using different systems. The zircon U/Pb age (25.23 ± 0.09 Ma) of the late metaluminous phase of the Cañada Pinabete pluton is identical to the sanidine $^{40}Ar/^{39}Ar$ age (25.23 ± 0.05 Ma) of the Amalia Tuff reported by Zimmerer (2008) calculated using the Renne et al. (1998) value for the Fish Canyon Tuff and the $^{40}K$ decay constant proposed by Steiger and Jäger (1977). Using the updated standard value (Kuiper et al., 2008) and $^{40}K$ decay constant (Min et al., 2000) the Amalia Tuff yields an older age (25.39 ± 0.05 Ma) than the late metaluminous phase of the pluton. However, because the peralkaline phase of the Cañada Pinabete is thought to be older than the late metaluminous phase it is plausible that the peralkaline phase is the same age as the Amalia Tuff (Hagstrum and Lipman, 1986). Unfortunately, the peralkaline phase has yielded no datable zircon and has a very poorly known $^{40}Ar/^{39}Ar$ date (K-spar inverse isochron 25.6 ± 0.7 Ma; Zimmerer, 2008). Although the available geochronology cannot directly establish an age correlation between the peralkaline phase of the Cañada Pinabete pluton and the Amalia Tuff, they are consistent with the correlation of the two made on the basis of nearly identical chemistry (Johnson and Lipman 1988; Johnson et al., 1989).

## 5.5 Evaluating fractional crystallization models for the Rio Hondo pluton

Johnson et al. (1989) proposed that most compositional variations within individual Latir intrusive units could be generated through fractional crystallization combined with filter pressing, and additionally suggested potential crystal fractionation

relationships between map units. Within the Rio Hondo pluton, the granitic roof was interpreted to have been fractionated/filter pressed from the more mafic roots in a two-stage process. The first stage involved derivation of "typical" granodiorite from "mafic" granodiorite, followed by a second stage from "typical" granodiorite to granite. The new geochronologic data presented here directly contradict this model.

Within the Rio Hondo pluton, the structurally highest granite crystallized before either of the structurally lower granodiorite units – precisely opposite the predicted age relationship. If the Rio Hondo pluton was incrementally assembled, as the geochronology, filling rates, and cooling rates all suggest, then no chemical relationship is expected between the granite and granodiorite, and fits of the geochemical data to a fractionation model is likely the result of an over-determined model.

## 5.6 Evaluating fractional crystallization trends between plutonic and volcanic rocks

Pluton-building caldera models require ignimbrites and remnant plutons to evolve *via* fractionation from the same parental magma body (Fig. 1.1-B; Hildreth, 2004; Lipman 2007). These models generally envision fractionating magma chambers with high-silica caps evolving above more mafic granodiorite roots (e.g., Hildreth, 1981; Bachmann and Bergantz, 2008b), much like the Johnson et al. (1989) model for the Rio Hondo granite. Although the data presented here rule out this possibility for the Rio Hondo itself, it is possible to compare the potential fractionation trends in the intrusive rocks as outlined by Johnson et al. (1989) to determine if the geochemistry of any of the exposed plutonic and volcanic rocks appear to be related through fractionation.

To investigate possible *in situ* geochemical evolution of the plutonic rocks, a simple trace-element equilibrium crystallization model was constructed. The proposed fractionation relationship investigated here is whether the peralkaline granite of the Cañada Pinabete pluton could be derived by fractionation/filter pressing of the early metaluminous magma (Johnson et al., 1989). Since the major, trace, and rare-earth element chemistry of the peralkaline granite is essentially indistinguishable from the Amalia Tuff it is interpreted to be unerupted ignimbrite (Lipman, 1988; Johnson et al., 1989). Therefore, understanding the chemical relationship within the Cañada Pinabete pluton is paramount to understanding the genetic relationship between the pluton and the ignimbrite.

To illustrate the trend that this fractionation assemblage would produce the model was calculated at 10, 20, 30, 40, 50, 70, and 90% crystals using the same geochemistry, modal mineral abundances, and fractionation relationship described by Johnson et al. (1989). The mineral partition coefficients proposed by Johnson et al. (1989) calculated using the data of Dillet and Czamanske (1987), however, are not used. Because no glass is preserved within the Questa plutonic rocks, the composition of the melt at the time of mineral formation is unknown, and the partition coefficients used by Johnson et al. (1989) were calculated from whole-rock and mineral data. Instead of these coefficients, those established by Bachmann et al. (2005) for the Fish Canyon Tuff calculated from mineral and glass compositions are used. Although using calculated values from another locality is not ideal, this compromise seems reasonable for several reasons. The Fish Canyon Tuff is comparable in bulk chemistry and modal mineralogy to the calc-alkaline plutonic rocks in the Latir field (Whitney and Stormer, 1985; Johnson et al., 1989).

Partition coefficients can vary significantly in high-silica melts (Mahood and Hildreth, 1983; Nash and Crecraft, 1985); consequently it is dubious to assume that any one set of coefficients is applicable to the entire crystallization of a magma. Finally, I do not seek any quantitative fractionation model, only an evaluation of differentiation trends. Whereas the magnitude of the partition coefficients for the Fish Canyon Tuff may be inappropriate for the Questa plutonic rocks, the direction of fractionation vectors should be the same.

An important caveat in Johnson et al. (1989) fractionation model is the potential role of halogen-rich fluid fluxes. While this process could alter the chemistry of the rocks during fractionation it is impossible to quantify, so it cannot be modeled. However, the bases on which Johnson et al. (1989) suggest halogen-fluxes occur and the effect this mechanism would have on specific elements is unclear. Thus it appears that halogen-rich fluid fluxes could be an example of a mechanism introduced so the data better fits the over-determined model. Regardless, these authors do not suggest that this mechanism occurs ubiquitously throughout the Latir field, so my objective of comparing the fractionation trends of plutonic and volcanic rocks does not appear to be comprised.

Results from the fractionation model (Fig. 5.2) demonstrate three key points: 1) Latir plutonic and volcanic rocks generally overlap and do not display the systematic difference in trace-element compositions observed between melt and residue in the model. 2) The trend of the model fractionation vector for the elements examined is oblique in reference to the overall trend of plutonic and volcanic rocks. Clearly the fractionation vector would change in angle, magnitude, and direction using different mineral assemblages, partition coefficients, and parent magma; yet nearly all Latir

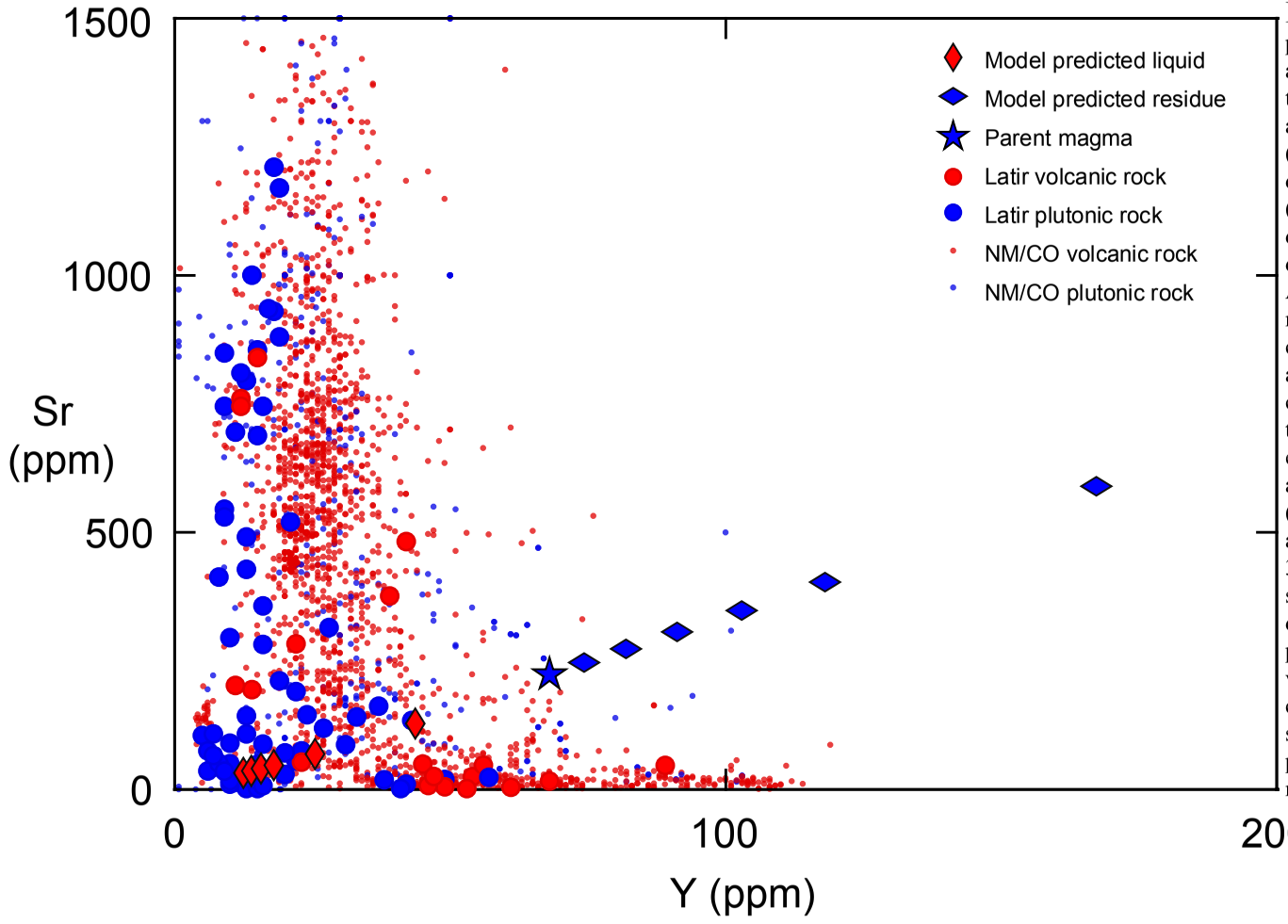


**Fig. 5.2**: Strontium vs. yttrium plot for the plutonic (blue circles) and volcanic rocks (red circles) of the Latir field (data from Johnson et al. 1989) and the Cenozoic plutonic (blue dots) and volcanic rocks (red dots) for New Mexico and Colorado (available in the NAVDAT database). Other trace elements demonstrate the same general trend. Also plotted are crystallization model predictions of expected crystal residues (blue diamonds) and liquid (red diamonds) compositions for fractionation of the peralkaline granite from an early metaluminous melt (blue star) as proposed by Johnson et al. (1989). The model was calculated at different crystallization (10, 20, 30, 40, 50, 70, 90% volume of melt) stages. See text for additional discussion of model setup and parameters. The plutonic and volcanic rocks contain similar compositions and do not display the systematic compositional difference predicted in the crystallization model.

plutonic and volcanic rocks plot along the same general trend. 3) It appears the trace element geochemistry of the peralkaline granite could be generated by fractionation of early metaluminous magma; however, this would also produce crystal residues with compositions unlike any found in the Latir rocks.

## 5.7 Top-down pluton construction

It appears the compositional variations within Latir plutons do not result from magma chamber differentiation, but instead represent sequential intrusion of compositionally distinct magmas. Within the Cañada Pinabeté pluton, field, paleomagnetic, and petrologic studies suggest the structurally highest peralkaline phase crystallized before the early metaluminous phase and structurally deepest late metaluminous phase (Hagstrum and Lipman, 1986; Johnson et al., 1986; Lipman, 1988). If the structurally highest, peralkaline phase of the pluton is unerupted Amalia Tuff (Lipman, 1988; Johnson et al., 1989), then it must have formed contemporaneously with the tuff (25.39 ± 0.05 Ma). Therefore the updated standard (Kuiper et al., 2008) and decay constant values (Min et al., 2000) suggest the peralkaline granite is older than the metaluminous granite (25.23 ± 0.09 Ma), which is consistent with the sequence of magma intrusion. Thus, available data suggest that the Cañada Pinabeté was built from the top downward.

Top down construction of the Rio Hondo pluton also seems likely. Zircon geochronology on the Rio Hondo pluton demonstrates that the granite (22.99 ± 0.12 Ma), the structurally highest sample, yields the oldest age, and the structurally lower granodiorite (22.81 ± 0.06; 22.63 ± 0.03; 22.49 ± 0.04 Ma) samples yield younger ages. These ages are consistent with incremental downward-stacking assembly of the pluton.

A growing number of examples suggest that downward-stacking of intrusions may be a common assembly sequence. High-precision geochronology and field relations suggest that the Tuolumne (Coleman et al., 2008) and Whitney (Hirt, 2007) intrusive suites of the Sierra Nevada Batholith, the Trachyte Mesa Laccolith of the Henry Mnts. (Morgan et al., 2008), and Torres Del Paine (Michel et al., 2008) along with other South American Cordilleran plutons (Cruden et al., 2005) are all downward-stacked sill-type intrusions.

Recent experimental studies and modeling predict downward stacking as a dominant mode of incremental pluton assembly (Kavanagh et al., 2006; Menand, 2008). These experiments demonstrate that magma rising along dikes will stall at rheological boundaries. Rising magma then spreads laterally at the boundary, and sill or laccolith formation is likely to occur. In the Cañada Pinabete and Rio Hondo plutons, after intrusion of the peralkaline and granite magmas (respectively), these units may have acted as rheological barriers, trapping later metaluminous and granodiorite pulses below. The rheological barriers may have formed either because the initial intrusions crystallized quickly, becoming a cohesive unit that resists fracturing, or because the sill contained melt when the next pulse of magma intruded (Coleman et al., 2008). If significant melt was still present, brittle deformation necessary for dike propagation is unlikely to have occurred when the next magma pulse intruded, thus trapping later pulses below earlier ones (Bacon et al., 1980; Wiebe and Collins, 1998).

## 5.8 Caldera model reevaluation

Differences between the pluton-building and non-pluton-building end-member caldera models are most clearly observed in two ways: 1) the volume of plutonic rocks

estimated to form contemporaneously with ignimbrite eruption (Fig 1.1-A) and 2) the predicted chemical relationship if plutonic rocks and volcanic rocks are related by crystal fractionation (Fig 1.1-B). Geochronology of the Latir plutons indicates the Cañada Pinabeté and Virgin Canyon plutons are the only plutons that may have formed synchronously with the ignimbrite, although using updated standard (Kuiper et al., 2008) and $^{40}K$ decay constant (Min et al., 2000) values it appears the Amalia Tuff is older than the metaluminous phases of the plutons. Thus, only the small (total exposure <10 $km^2$) peralkaline phase of the plutons is permissibly the same age as the tuff. This unit is preserved dominantly as thin dikes and a small capping unit, not as a large volume residue. These observations are much more consistent with the predictions of the non-pluton building model for caldera formation.

Geochemistry indicates that the peralkaline phase of the Cañada Pinabete pluton and the Amalia Tuff are essentially identical, leading previous workers to conclude that they were plutonic/volcanic equivalents (Lipman, 1988; Johnson et al., 1989). This observation is also most consistent with the non-pluton-building model for calderas – the units are chemically indistinguishable, not crystal/liquid pairs. Considering the Latir field as a whole, trace-element modeling indicates that none of the plutonic and volcanic rocks are likely to be related by crystal fractionation of the phases present in the plutonic rocks. Thus again, it appears the non-pluton-building caldera model seems more appropriate for the Questa caldera.

Two important caveats to the arguments presented against the pluton-building caldera model should be considered. First, only a small fraction of the plutonic rocks likely to be preserved under the Questa caldera are exposed. What if the coeval

cumulates of the Amalia Tuff are preserved at deeper, unexposed structural levels? Second, could the fraction of liquid withdrawn from the magma chamber during eruption of the Amalia Tuff be so small that its removal could be masked by a large intrusive:extrusive rock ratio?

The Questa caldera sits above a regional gravity anomaly inferred to result from a composite batholith (Cordell et al., 1985; Long, 1985). This batholith is proposed to represent the source from which the Amalia Tuff was generated (Lipman, 1988; Johnson et al., 1989; Lipman 2007). Gravity lows are commonly found in the subsurface beneath caldera systems (e.g. Davy and Caldwell, 1998; Marti et al., 2008), and whereas some interpretations suggest they represent the plutonic rock from which the ignimbrite was fractionated (Lipman, 2007), others suggest these anomalies reflect the presence of post-caldera (waning stage) intrusions (Steck et al., 1998).

Although it is not presently possible to know the geochemistry, petrology or age of the inferred batholith under the Questa caldera, it seems reasonable to expect that if this gravity anomaly results from a voluminous crystal cumulate then these cumulates should be exposed in other volcanic systems. However, consideration of other plutonic and volcanic Cenozoic rocks in New Mexico and Colorado available on the NAVDAT database reveals that few samples are likely fractionation residues (Fig. 5.2). Instead, expansion of the data inquiry beyond the Latir field reinforces the observation that the chemistry of plutonic and volcanic rocks is essentially identical (Mills et al., 2008). It appears that either fractionation residua are suspiciously absent in rocks exposed in the dataset or *in situ* fractionation may not be the process that determines the chemistry of these rocks.

However it is possible to dilute the effect of shallow fractionation in the chemistry of sub-caldera plutonic rocks if these rocks are generated in systems with very high intrusive:extrusive rock ratios (Lipman, 2007). The inferred batholith at Questa is approximately equal in size to the ignimbrite (500 $km^3$) and therefore yields a ratio of approximately 1:1 (Cordell et al., 1985). This ratio is significantly less than the most prominently cited 10:1 ratio (Smith, 1979), but compares more favorably to lower ratios (2-3:1) proposed in recent work (White et al., 2006). These low intrusive:extrusive ratios are not conducive to hiding the geochemical signature of melt extraction in plutonic rocks. In fact, as the ratio converges on low estimates (e.g. 1:1 Latir ratio), the problem is exacerbated. Thus it appears that the intrusive:extrusive rock ratio of the Latir field is not sufficiently high enough to dilute the effect of fractionation.

If the chemistry of plutonic and volcanic rocks of the Latir and southern Rocky Mountain region is not controlled by upper-crustal crystal fractionation then what is the origin of the high-silica rocks? I suggest that the magmas that form the Latir rocks could be derived from basaltic sources in the lower crust and chemical diversity is inherited at the time of formation, consistent with crystal residues not found in the upper-crust.

Experimental petrology demonstrates that high-silica rocks can be produced by melting of basaltic sources in the deep crust (Sisson et al., 2005). Annen et al. (2006) propose that most arc magmas are derived in the lower crust, primarily by partial crystallization of basalt sills (generated by decompression melting of mantle wedge) and melting of pre-existing crustal rock. While the Latir rocks are derived from rift-related processes, the low trace-element concentrations are typical of cold-wet arc-related magmas (Bachmann and Bergantz, 2008b). This distinction is notable since water

content promotes the melting of crustal rocks. Following derivation in the lower-crust, compositionally evolved silicic magma pulses ascend to shallow crustal levels where crystallization occurs rapidly and little alteration occurs to the chemistry of the melt. Subsequent pulses intruded along the same conduit plane will likely stall structurally below prior intrusions forming plutons constructed from the top-downward (Kavanagh et al., 2006; Menand, 2008). Thus chemical heterogeneities within individual plutons (e.g. Rio Hondo granite and Rio Hondo granodiorite) may record multiple magma pulses derived from a slight variance of the source material.

I propose that data and observation are converging on the interpretation that eruption of the Amalia Tuff resulted in nearly complete evacuation of the ignimbrite magma chamber, now preserved only as small sheets of peralkaline rocks. This proposal is consistent with modeling experiments that suggest total magma chamber evacuation can occur during eruptions (Roche and Druitt, 2001; Geyer et al., 2006). Theoretical calculations demonstrate that in some calderas (e.g. Pinatubo, Vesuvius) nearly 90% of the magma chamber must have erupted to trigger roof collapse. The percentage of magma chamber withdrawal is dependant on roof aspect ratio, collapse style, and magma chamber depth, and is highly variable with values as low as 10% (Fig. 5 from Roche and Druitt, 2001). However these are the minimum values needed to trigger eruption, so a greater percentage of the chambers could evacuate during eruption.

# 6. CONCLUSIONS

New zircon U/Pb geochronology, combined with existing $^{40}Ar/^{39}Ar$ geo- and thermochronology (Zimmerer, 2008), establish the history of plutonism and volcanism within the Latir volcanic field. Zircon U/Pb geochronology demonstrates that the peralkaline phase of the Cañada Pinabete potentially formed synchronously with the Amalia Tuff, whereas the metaluminous phase of the Cañada Pinabete, the Cabresto Lake and Rio Hondo plutons formed during the post-caldera, waning phase of magmatism. However, direct correlation of plutonic/volcanic rock pairs is limited by the precision of decay constants, though advances in the accuracy and precision of decay constants (e.g. Min et al., 2000) and standards (e.g. Kuiper et al., 2008) provide some cautious optimism.

Pluton filling rates for the Rio Hondo and other examples from the literature with well-established pluton-building timescales are significantly slower than modeled pluton filling rates presented by Petford et al. (2000). We suggest that pluton filling rates will be overestimated if episodic assembly is overlooked. Incremental assembly of the Rio Hondo pluton also resulted in a protracted cooling history not evident in the smaller plutons investigated here.

The Canada Pinabete and Rio Hondo plutons appear to be examples of top-down pluton construction. Within the Rio Hondo pluton, the structurally highest granite yields a zircon U/Pb age 500 K.y. older than the youngest and structurally lower granodiorite sample. The span of zircon ages, slow filling rates, and protracted cooling rates are

consistent with top-down incremental pluton construction, and directly contradict fractional crystallization as the process that creates the compositional variations found within the pluton.

Examination of fractionation models for differentiation of the plutonic and volcanic rocks reveals significant problems. Although complicated models for fractionation can be made to fit the data, geochronologic data contradict the most basic assumptions of the models – derivative liquids in the Rio Hondo pluton are demonstrably older than the inferred parent. Consideration of available geochemical data for all the plutonic and volcanic rocks within the Latir and throughout the Cenozoic rocks of New Mexico and Colorado show no systematic differences that might be expected if the rocks represent residue and liquid derived from "big tank" magma chambers.

The non-pluton-building model appears to best depict the Questa caldera. Although it is possible that big crystal cumulates underlie the exposed plutons, the important observations that 1) there is a small exposed pluton phase similar in age and chemistry to the Amalia Tuff, and 2) there is no systematic difference in the chemistry of plutonic and volcanic rocks across the entire field, lead me to conclude that there is no compelling reason to favor the pluton-building model. Instead, existing data all support a non-pluton-building model, so it should not be discarded, and may apply to other caldera system.

## REFERNCES


Annen, C., Blundy, J. D., and Sparks, R. S. J., 2006, The genesis of intermediate and silicic magmas in deep crustal hot zones: Journal of Petrology, v. 47, no. 3, p. 505-539.

Audi, G., Bersillon, O., Blachot, J., and Wapstra, A. H., 1997, The NUBASE evaluation of nuclear and decay properties: Nuclear Physics A, v. 624, no. 1, p. 1-124.

Bachl, C. A., Miller, C. F., Miller, J. S., and Faulds, J. E., 2001, Construction of a pluton; evidence from an exposed cross section of the Searchlight Pluton, Eldorado Mountains, Nevada: Geological Society of America Bulletin, v. 113, no. 9, p. 1213-1228.

Bachmann, O., and Bergantz, G. W., 2003, Rejuvenation of the Fish Canyon magma body; a window into the evolution of large-volume silicic magma systems: Geology, v. 31, no. 9, p. 789-792.

-, 2004, On the origin of crystal-pore rhyolites extracted from batholithic crystal mushes: Journal of Petrology, v. 45, no. 8, p. 1565-1582.

-, 2008a, The magma reservoirs that feed supereruptions: Elements, v. 4, no. 1, p. 17-21.

-, 2008b, Rhyolithes and their Source Mushes across Tectonic Settings: Journal of Petrology, v. 49, no. 12, p. 2277-2285.

Bachmann, O., Dungan, M. A., and Bussy, F., 2005, Insights into shallow magmatic processes in large silicic magma bodies; the trace element record in the Fish Canyon magma body, Colorado: Contributions to Mineralogy and Petrology, v. 149, no. 3, p. 338-349.

Bachmann, O., Dungan, M. A., and Lipman, P. W., 2000, Voluminous lava-like precursor to a major ash-flow tuff; low-column pyroclastic eruption of the Pagosa Peak Dacite, San Juan volcanic field, Colorado: Journal of Volcanology and Geothermal Research, v. 98, no. 1-4, p. 153-171.

Bachmann, O., Miller, C. F., and Silva, S. L. d., 2007a, The volcanic-plutonic connection as a stage for understanding crustal magmatism: Journal of Volcanology and Geothermal Research, v. 167, no. 1-4, p. 1-23.

Bachmann, O., Oberli, F., Dungan, M. A., Meier, M., Mundil, R., and Fisher, H., 2007b, 40Ar/39Ar and U/Pb dating of the Fish Canyon magmatic system, San Juan volcanic field, Colorado; evidence for an extended crystallization history: Chemical Geology, v. 236, no. 1-2, p. 134-166.

Bacon, C. R., Duffield, W. A., Nakamura, K., 1980, Distribution of Quaternary rhyolite domes of the Coso Range, California; implications for extent of the geothermal anomaly: Journal of Geophysical Research, v. 85, no. B5, p. 2425-2433.

Bartley, J. M., Coleman, D. S., and Glazner, A. F., 2005, Incremental pluton emplacement by magmatic crack-seal: Transactions of the Royal Society of Edinburgh: Earth Sciences, v. 97, no. 4, p. 383-396.

Chapin, C., E., 1979, Evolution of the Rio Grande Rift; a summary, in Riecker, R. E., ed., Rio Grande Rift; tectonics and magmatism, p. 1-5.

Coleman, D. S., Davis, J. W., Bartley, J. M., and Glazner, A. F., 2008, Downward-stacking laccoliths, in LASI III Conference, Elba Island.

Coleman, D. S., Gray, W., and Glazner, A. F., 2004, Rethinking the emplacement and evolution of zoned plutons; geochronologic evidence for incremental assembly of the Tuolumne Intrusive Suite, California: Geology, v. 32, no. 5, p. 433-436.

Cordell, L., Long, C. L., and Jones, D. W., 1985, Geophysical expression of the batholith beneath Questa Caldera, New Mexico: Journal of Geophysical Research, v. 90, no. B13, p. 11,263-11,269.

Cruden, A. R., 2006, Emplacement and growth of plutons; implications for rates of melting and mass transfer in continental crust, in Brown, M., and Rushmer, T., eds., Evolution and differentiation of the continental crust, p. 455-519.

Cruden, A. R., Grocott, J., McCaffrey, K. J. W., and Davis, D. D., 2005, Timescales of incremental pluton growth; theory and a field-based test: Abstracts with Programs - Geological Soceity of America, v. 37, no. 7, p. 131.

Cruden, A. R., and McCaffrey, K. J. W., 2001, Growth of plutons by floor subsidence; implications for rates of emplacement, intrusion spacing and melt-extraction mechanisms: Physics and chemistry of the earth. Part A, Solid earth and geodesy, v. 26, no. 4-5, p. 303-315.

Czamanske, G. K., Foland, K. A., Kubacher, F. A., and Allen, J. C., 1990, The $^{40}Ar/^{39}Ar$ chronology of caldera formation, intrusive activity and Mo-ore deposition near Questa, New Mexico, in Bauer, P. W., Lucas, S. G., Mawer, C. K., and McIntosh, W. C., eds., Guidebook- New Mexico Geological Society, p. 355-358.

Davy, B. W., and Caldwell, T. G., 1998, Gravity, magnetic, and seismic surveys of the caldera complex, Lake Taupo, North Isand, New Zealand: Journal of Volcanology and Geothermal Research, v. 81, no. 1-2, p. 69-89.

de Silva, S. L., Bachmann, O., Miller, C. F., Yoshida, T., Knesel, K., and eds, 2007, Preface to Large Silicic Magmatic Systems: Special Volume of the Journal of Volcanology and Geothermal Research, v. 167, p. vii-ix.

de Silva, S. L., and Gosnold, W. D., 2007, Episodic construction of batholiths; insights from the spatiotemporal development of an ignimbrite flare-up: Journal of Volcanology and Geothermal Research, v. 167, no. 1-4, p. 320-335.

Dillet, B., and Czamanske, G. K., 1987, Aspects of the petrology, mineralogy, and geochemistry of the granitic rocks associated with Questa Caldera, northern New Mexico: U.S. Geological Survey, OF 87-0258.

Dodson, M. H., 1973, Closure Temperature in Cooling Geochronological and Petrological Systems: Contributions to Mineralogy and Petrology, v. 40, no. 3, p. 259-274.

Druitt, T. H., and Bacon, C. R., 1989, Petrology of the zoned calcalkaline magma chamber of Mount Mazama, Crater Lake, Oregon: Contributions to Mineralogy and Petrology, v. 101, no. 2, p. 245-259.

Eichelberger, J. C., Izbekov, P. E., and Browne, B. L., 2006, Bulk chemical trends at arc volcanoes are not liquid lines of descent: Lithos, v. 87, no. 1-2, p. 135-154.

Geyer, A., Folch, A., and Marti, J., 2006, Relationship between caldera collapse and magma chamber withdrawal: An experimental approach: Journal of Volcanology and Geothermal Research, v. 157, no. 4, p. 375-386.

Glazner, A. F., 1991, Plutonism, oblique subduction, and continental growth; an example from the Mesozoic of California: Geology, v. 19, no. 8, p. 784-786.

Glazner, A. F., Bartley, J. M., Coleman, D. S., Gray, W., and Taylor, R. Z., 2004, Are plutons assembled over millions of years by amalgamation from small magma chambers? GSA Today, v. 14, no. 4-5, p. 4-11.

Glazner, A. F., Coleman, D. S., and Bartley, J. M., 2008, The tenuous connection between high-silica rhyolites and granodiorite plutons: Geology, v. 36, no. 2, p. 183-186.

Gracely, J. T., 2007, Rapid pluton emplacement via multiple discrete pulses, Lamarck granodiorite, central Sierra Nevada Batholith, California [Thesis]: University of North Carolina at Chapel Hill, 89 p.

Hagstrum, J.T., and Lipman, P.W., 1986, Paleomagnetism of the structurally deformed Latir volcanic field, northern New Mexico: relations to formation of the Questa caldera and development of the Rio Grande rift: Journal of Geophysical Research, v. 91, no. B7, p. 7383-7402.

Hanson, R. B., and Glazner, A. F., 1995, Thermal requirements for extensional emplacement of granitoids: Geology, v. 23, no. 3, p. 213-216.

Harrison, T. M., Duncan, I., and McDougall, I., 1985, Diffusion of 40Ar in biotite; temperature, pressure and compositional effects: Geochimica et Cosmochimica Acta, v. 49, no. 11, p. 2461-2468.

Hildreth, W., 1981, Gradients in silicic magma chambers; implications for lithospheric magmatism: Journal of Geophysical Research, v. 86, no. B11, p. 10153-10192.

-, 2004, Volcanological perspectives on Long Valley, Mammoth Mountain, and Mono Craters; several contiguous but discrete systems: Journal of Volcanology and Geothermal Research, v. 136, no. 3-4, p. 169-198.

Hirt, W. H., 2007, Petrology of the Mount Whitney Intrusive Suite, eastern Sierra Nevada, California; implications for the emplacement and differentiation of composite felsic intrusions: Geological Society of America Bulletin, v. 119, no. 9-10, p. 1185-1200.

Holm, D. K., and Dokka, R. K., 1993, Interpretation and tectonic implications of cooling histories; an example from the Black Mountains, Death Valley extended terrance, California: Earth and Planetary Science Letters, v. 116, no. 1-4, p. 63-80.

Ivanov, A. V., 2006, Systematic differences between U-Pb and Ar-40/Ar-39 dates: Reasons and evaluation techniques: Geochemistry International, v. 44, no. 10, p. 1041-1047.

Jaffey, A. H., Flynn, K. F., Glendenin, L. E., Bentley, W. C., and Essling, A. M., 1971, Precision measurement of half-lives and specific activities of 235U and 238U: Physical Review C, v. 4, no. 5, p. 1889-1906.

Johnson, C. M., Czamanske, G. K., and Lipman, P. W., 1989, Geochemistry of intrusive rocks associated with the Latir volcanic field, New Mexico, and contrasts between evolution of plutonic and volcanic rocks: Contributions to Mineralogy and Petrology, v. 103, no. 1, p. 90-109.

Johnson, C. M., and Lipman, P. W., 1988, Origin of metaluminous and alkaline volcanic rocks of the Latir volcanic field, northern Rio Grande Rift, New Mexico: Contributions to Mineralogy and Petrology, v. 100, no. 1, p. 107-128.

Johnson, C. M., Lipman, P. W., and Czamanske, G. K., 1991, H, O, Sr, Nd, and Pb isotope geochemistry of the Latir volcanic field and cogenetic intrusions, New Mexico, and relations between evolution of a continental magmatic center and modifications of the lithosphere: Contributions to Mineralogy and Petrology, v. 104, no. 1, p. 99-124.

Kavanaugh, J.L., Menand, T., Sparks, R.S.J., 2006, An experimental investigation of sill formation and propagation in layered elastic media: Earth and Planetary Science Letters, v. 245, no. 3-4, p. 799-813.

Kossert, K., and Gunther, E., 2004, LSC measurements of the half-life of K-40: Applied Radiation and Isotopes, v. 60, no. 2-4, p. 459-464.

Krogh, T. E., 1973, A low-contamination method for hydrothermal decomposition of zircon and extraction of U and Pb for isotopic age determinations: Geochimica et Cosmochimica Acta, v. 37, no. 3, p. 485-494.

Krumrei, T. V., Villa, I. M., Marks, M. A. W., and Markl, G., 2006, A 40Ar/39Ar and U/Pb isotopic study of the Ilimaussaq Complex, South Greenland; implications for the 40K decay constant and for the duration of magmatic activity in a peralkaline complex: Chemical Geology, v. 227, no. 3-4, p. 258-273.

Kuiper, K. F., Deino, A., Hilgen, F. J., Krijgsman, W., Renne, P. R., and Wijbrans, J. R., 2008, Synchronizing rock clocks of Earth history: Science, v. 320, no. 5875, p. 500-504.

Leonardson, R. W., Dunlop, G., Starquist, V. L., Bratton, G. P., Meyer, J. W., and Osborne, L. W. J., 1983, Preliminary geology and molybdenum deposits at Questa, New Mexico, in Proceedings of the Denver Region Exploration Geologists Society symposium; the genesis of Rocky Mountain ore deposits; changes with time and tectonics, Denver, CO, p. 151-155.

Lipman, P. W., 1984, The roots of ash flow calderas in western North America; windows into the tops of granitic batholiths: Journal of Geophysical Research, v. 89, no. B10, p. 8801-8841.

-, 1988, Evolution of silicic magma in the upper crust; the mid-Tertiary Latir volcanic field and its cogenetic granitic batholith, northern New Mexico, U.S.A.: Transactoins of the Royal Society of Edinburgh: Earth Sciences, v. 79, no. 2-3, p. 265-288.

-, 2007, Incremental assembly and prolonged consolidation of Cordilleran magma chambers; evidence from the Southern Rocky Mountain volcanic field: Geosphere, v. 3, no. 1, p. 42-70.

Lipman, P. W., Mehnert, H. H., and Naeser, C. W., 1986, Evolution of the Latir volcanic field, northern New Mexico, and its relation to the Rio Grande Rift, as indicated by potassium-argon and fission track dating: Journal of Geophysical Research, v. 91, no. B6, p. 6329-6345.

Lipman, P. W., and Reed, J.C. Jr., 1989, Geologic Map of the Latir volcanic field and adjacent areas, northern New Mexico: U.S. Geological Survey, Miscellaneous Map 1 1907, scale 1:48,000.

Long, C. L., 1985, Regional audiomagnetotelluric study of the Questa Caldera, New Mexico: Journal of Geophysical Research, v. 90, no. B13, p. 11,270-11,274.

Mahood, G., and Hildreth, W., 1983, Large partition coefficients for trace elements in high-silica rhyolites: Geochimica et Cosmochimica Acta, v. 47, no. 1, p. 11-30.

Marti, J., Geyer, A., Folch, A., Gottsmann, J., 2008, A review on collapse caldera modeling, in Gottsmann, J., and Marti, J., eds., Caldera volcanism: analysis, modeling and response, p. 233-284.

Mattinson, J. M., 2005, Zircon U/Pb chemical abrasion (CA-TIMS) method; combined annealing and multi-step partial dissolution analysis for improved precision and accuracy of zircon ages: Chemical Geology, v. 220, no. 1-2, p. 47-66.

Matzel, J. E. P., Bowring, S. A., and Miller, R. B., 2006, Time scales of pluton construction at differing crustal levels; examples from the Mount Stuart and Tenpeak Intrusions, north Cascades, Washington: Geological Society of America Bulletin, v. 118, no. 11-12, p. 1412-1430.

McDougall, I., and Harrison, T. M., 1989, Geochronology and thermochronology by the 40Ar/39Ar method: Oxford, United Kingdom, Oxford University Press.

Menand, T., 2008, The mechanics and dynamics of sills in layered elastic rocks and their implications for the growth of laccoliths and other igneous complexes: Earth and Planetary Science Letters, v. 267, no. 1-2, p. 93-99.

Meyer, J., and Foland, K. A., 1991, Magmatic-tectonic interaction during early Rio Grande Rift extension at Questa, New Mexico: Geological Society of America Bulletin, v. 103, no. 8, p. 993-1006.

Meyer, J. W., 1991, Volcanic, plutonic, tectonic and hydrothermal history of the southern Questa Caldera, New Mexico [dissertation thesis]: University of California at Santa Barbara, 348 p.

Michel, J., Baumgartner, L., Putlitz, B., Schaltegger, U., and Ovtcharova, M., 2008, Incremental growth of the Patagonian Torres del Paine Laccolith over 90 k.y.: Geology, v. 36, no. 6, p. 459-462.

Miller, C. F., Meschter McDowell, S., and Mapes, R. W., 2003, Hot and cold granites? Implications of zircon saturation temperatures and preservation of inheritance: Geology, v. 31, no. 6, p. 529-532.

Mills, R. D., Glazner, A. F., Coleman, D. S., 2008, Comparing the compositional patterns of volcanic and plutonic rocks using the NAVDAT database: Geochimica et Cosmochimica Acta, v. 72, no. 12S, p. A631.

Min, K., Mundil, R., Renne, P. R., and Ludwig, K. R., 2000, A test for systematic errors in 40Ar/39Ar geochronology through comparison with U/Pb analysis of a 1.1-Ga rhyolite: Geochimica et Cosmochimica Acta, v. 64, no. 1, p. 73-98.

Morgan, S., Stanik, A., Horsman, E., Tikoff, B., de Saint Blanquat, M., Habert, G., 2008, Emplacement of multiple magma sheets and wall rock deformation: Trachyte Mesa intrusion, Henry Mountains, Utah: Journal of Structural Geology, v. 30 no. 4, p. 491-512.

Mundil, R., Ludwig, K. R., Metcalfe, I., and Renne, P. R., 2004, Age and timing of the Permian mass extinctions; U/Pb dating of closed-system zircons: Science, v. 305, no. 1760-1763.

Nash, W. P., and Crecraft, H. R., 1985, Partition coefficients for trace elements in silicic magmas: Geochimica et Cosmochimica Acta, v. 49, no. 11, p. 2309-2322.

Oberli, F., Fisher, H., and Meier, M., 1990, High-resolution 238U/206Pb zircon dating of Tertiary bentonites and Fish Canyon Tuff; a test for age "concordance" by single-crystal analysis, in Seventh international conference on Geochronology, cosmochronology, and isotope geology; abstracts volume, Canberra, Australia, p. 74.

Parrish, R. R., and Krogh, T. E., 1987, Synthesis and purification of 205Pb for U-Pb geochronology: Chemical Geology; Isotope Geosciences Section, v. 66, no. 1-2, p. 103-110.

Petford, N., Cruden, A. R., McCaffrey, K. J. W., and Vigneresse, J. L., 2000, Granite magma formation, transport and emplacement in the Earth's crust: Nature, v. 408, no. 6813, p. 669-673.

Renne, P.R., Swisher, C.C., Deino, A.L., Karner, D.B., Owens, T.L., and DePaolo, D.J., 1998, Intercalibration of standards, absolute ages and uncertainties in 40Ar/39Ar dating, Chemical Geology, v. 145, p. 117-152.

Roche, O., and Druitt, T. H., 2001, Onset of caldera collapse during ignimbrite eruptions: Earth and Planetary Science Letters, v. 191, no. 3-4, p. 191-202.

Schmitz, M. D., and Bowring, S. A., 2001, U-Pb zircon and titanite systematics of the Fish Canyon Tuff; an assessment of high-precision U-Pb geochronology and its application to young volcanic rocks: Geochimica et Cosmochimica Acta, v. 65, no. 15, p. 2571-2587.

Sisson, T. W., Ratajeski, K., Hankins, W. B., and Glazner, A. F., 2005, Voluminous granitic magmas from common basaltic sources: Contributions to Mineralogy and Petrology, v. 148, no. 6, p. 635-661.

Smith, G. A., Moore, J. D., and McIntosh, W. C., 2002, Assessing roles of volcanism and basin subsidence in causing Oligocene-lower Miocene sedimentation in the northern Rio Grande Rift, New Mexico, U.S.A.: Journal of Sedimentary Research, v. 72, no. 6, p. 836-848.

Smith, R.L., 1979, Ash-flow magmatism, in Chapin, C.E., and Elston, W.E., eds., Ash-flow Tuffs: Geological Society of America Special Paper 180, p. 5-27.

Steck, L. K., Thurber, C. H., Fehler, M. C., Lutter, W. J., Roberts, P. M., Baldridge, W. S., Stafford, D. G., and Sessions, R., 1998, Crust and upper mantle P wave velocity structure beneath Valles Caldera, New Mexico; results from the Jemez teleseismic tomography experiment: Journal of Geophysical Research, v. 103, no. B10, p. 24,301-24,320.

Steiger, R. H., and Jager, E., 1977, Subcommission on Geochronology; convention on the use of decay constants in geochronology and cosmochronology, in 25th International geological congress, Geological time scale symposium, Sydney, Australia, p. 67-71.

Thompson, R. A., Dungan, M. A., and Lipman, P. W., 1986, Multiple differentiation processes in early-rift calc-alkaline volcanics, northern Rio Grande Rift, New Mexico: Journal of Geophysical Research, v. 91, no. B6, p. 6046-6058.

Tweto, O., 1979, The Rio Grande rift system in Colorado, in Riecker, R. E., ed., Rio Grande Rift; tectonics and magmatism, p. 33-68.

Ulmer, P., Muntener, O., Kagi, R., Perez, R. A., and Villiger, S., 2007, Where do primative arc magmas differentitiate and acquire their major and trace element composition? An assessment based on field, geochemical and experimental data, in State of the Arc 2007, Termas Puyehue, Chile, p. 253-256.

Vigneresse, J. L., 1995, Control of granite emplacement by regional deformation: Tectonophysics, v. 249, no. 3-4, p. 173-186.

Watson, E. B., and Harrison, T. M., 1983, Zircon saturation revisited: temperature and composition effects in a variety of crustal magma types: Earth and Planetary Science Letters, v. 64, no. 2, p. 295-304.

White, S. M., Crisp, J. A., and Spera, F. J., 2006, Long-term volumetric eruption rates and magma budgets: Geochemistry, Geophysics, Geosystems - G3, v. 7, no. 3, p. 20.

Whitney, J. A., and Stormer, J. C. J., 1985, Mineralogy, petrology, and magmatic conditions from the Fish Canyon Tuff, central San Juan volcanic field, Colorado: Journal of Petrology, v. 26, no. 3, p. 726-762.

Wiebe, R. A., and Collins, W. J., 1998, Depositional features and stratigraphic sections in granitic plutons; implications for the emplacement and crystallization of granitic magma: Journal of Structural Geology, v. 20, no. 9-10, p. 1273-1289.

Wiebe, R. A., Smith, D., Strum, M., King, E. M., and Seckler, M. S., 1997, Enclaves in the Cadillac Mountain Granite (costal Maine); samples of hybrid magma from the base of the chamber: Journal of Petrology, v. 38, no. 3, p. 393-423.

Yoshinobu, A. S., Okaya, D. A., and Paterson, S. R., 1998, Modeling the thermal evolution of fault-controlled magma emplacement models; implications for the solidification of granitoid plutons: Journal of Structural Geology, v. 20, no. 9-10, p. 1205-1218.

Zimmerer, M. J., 2008, The $^{40}Ar/^{39}Ar$ geochronology and thermochronology of the Latir volcanic field and associated intrusions: implications for caldera-related magmatism, [Thesis]: New Mexico Institute of Mining and Technology, 113 p.